Voltage-dependent activation of Rac1 by $Na_v1.5$ channels promotes cell migration

Ming Yang[1], Andrew D. James[1,2], Rakesh Suman[3], Richard Kasprowicz[3], Michaela Nelson[1,2], Peter J. O'Toole[4] and William J. Brackenbury[1,2*]

[1]Department of Biology, University of York, Heslington, York, YO10 5DD, UK

[2]York Biomedical Research Institute, University of York, Heslington, York, YO10 5DD, UK

[3]Phase Focus Ltd, Electric Works, Sheffield Digital Campus, Sheffield, S1 2BJ, UK

[4]Bioscience Technology Facility, Department of Biology, University of York, Heslington, York, YO10 5DD, UK

Running title: Voltage-dependent migration via $Na_v1.5$ and Rac1

*Corresponding author:

Dr. William J. Brackenbury, Department of Biology and York Biomedical Research Institute, University of York, Heslington, York YO10 5DD, UK

Email: william.brackenbury@york.ac.uk

Tel: +44 1904 328284

Fax: +44 1904 328505

ORCID: 0000-0001-6882-3351

Keywords: Breast cancer / membrane potential / migration / $Na_v1.5$ / Rac1

Abstract

Changes in ion channel activity can regulate the plasma membrane potential (V_m) and alter cancer cell migration as a result of altered ion flux. However, the mechanism by which V_m regulates motility remains unclear. Here, using patch clamp recording, we show that the $Na_v1.5$ voltage-gated Na^+ channel carries a steady state inward persistent Na^+ current which reversibly depolarizes the resting V_m at the timescale of minutes. Immunocytochemistry and confocal microscopy reveal that this $Na_v1.5$-dependent V_m depolarization increases Rac1 colocalization with phosphatidylserine, to which it is anchored at the leading edge of migrating cells, promoting Rac1 activation. Combining a genetically-encoded FRET biosensor of Rac1 activation with morphological analysis shows that depolarization-induced Rac1 activation results in the acquisition of a motile mesenchymal-like cellular phenotype. By identifying $Na_v1.5$-mediated V_m depolarization as a regulator of Rac1 activation, we link ionic and electrical signaling at the plasma membrane to small GTPase-dependent cytoskeletal reorganization and cellular migration. We uncover a novel and unexpected voltage-dependent mechanism for Rac1 activation, which fine tunes cell migration in response to ionic and/or electric field changes in the local microenvironment.

Introduction

Cellular morphological changes and migration play key roles in normal physiological processes, including during embryonic development and tissue repair. On the other hand, dysfunctional migration occurs in many disease processes, including cancer metastasis [1]. In particular, mesenchymal migration, which is dependent on polarization and formation of lamellipodial protrusions at the leading edge of cells, enables carcinoma cells to escape from primary tumors into surrounding tissues [2].

Dynamic and adaptable changes in actin polymerization leads to altered stiffness, elongation and branching, which in turn permits acquisition of a mesenchymal phenotype and formation of lamellipodial protrusions [3]. These changes are tightly regulated by a multiplicity of signaling mechanisms which are coordinated by the Rho family of small GTPases [4]. One of the best studied Rho GTPases, Rac1, plays a critical role in regulating lamellipodia formation and migration [5]. Rac1 cycles between active (GTP-bound) and inactive (GDP-bound) forms, catalyzed by guanine nucleotide exchange factors (GEFs) and GTPase-activating proteins (GAPs), respectively [6]. Rac1 translocates between cytoplasmic and plasma membrane-bound compartments, with activation predominantly occurring at the plasma membrane [7]. Translocation of Rac1 to the plasma membrane and interaction with phospholipids precedes interaction with GEFs and nucleotide exchange/activation [8]. Rac1 is anchored to the inner leaflet of the plasma membrane through its prenylated C-terminus and polybasic motif [9], which permits interaction with the anionic phospholipids PIP2, PIP3 and phosphatidylserine [10-12]. Localized clustering of PIP2, PIP3 and phosphatidylserine within the plasma membrane thus permits precise spatial and temporal distribution of Rac1 activation [12-14]. Rac1 activation gradients within heterogeneous signaling nanodomains in turn regulate cytoskeletal rearrangement, lamellipodia formation and migration through binding to WASP-family verprolin-homologous (WAVE) proteins and activation of the actin-related protein 2/3 (Arp2/3) protein complex [12, 15-17]. However, despite its pivotal role in

migration, the cellular mechanisms regulating local Rac1 clustering at the plasma membrane are still incompletely understood.

Another set of proteins that play a key role in regulating cellular migration is ion channels [18]. Changes in ion channel expression and/or activity in cancer cells regulate the plasma membrane potential (V_m) and intracellular signaling cascades as a result of altered ion flux [19, 20]. Motile cancer cells possess a more depolarized V_m compared to terminally-differentiated non-cancer cells [21]. The V_m is functionally instructive in regulating cell cycle progression [22], proliferation [23, 24], differentiation [25], cytoskeletal reorganization [26-30], tissue morphogenesis, regeneration and tumorigenesis [31-37]. V_m depolarization controls mitogenic signaling by promoting redistribution of phosphatidylserine and PIP2 in the inner leaflet of the plasma membrane, enhancing nanoclustering and activation of the small GTPase K-Ras [24]. However, the mechanisms by which V_m regulates other behaviors, including morphological changes and migration, and the dependency of V_m alterations on ion channel activity, remain unclear.

An important class of ion channels in the context of cellular migration is the voltage-gated Na^+ channels (VGSCs). VGSCs contain a pore-forming α subunit ($Na_v1.1$-$Na_v1.9$), together with one or more smaller β subunits ($\beta1$-$\beta4$) [38, 39]. The canonical function of VGSCs is to regulate V_m depolarization during the rising phase of action potentials in electrically-excitable cells [40]. In addition, VGSCs not only regulate neuronal pathfinding and migration [41-43], but also regulate the migration of non-excitable cells [44]. For example, the $Na_v1.5$ subtype is upregulated in breast cancer cells where it plays a critical role in promoting cellular migration, invasion and metastasis [45-52]. In non-excitable cancer cells, $Na_v1.5$ carries a small persistent inward Na^+ current, which would be expected to depolarize the V_m at steady state [50, 53]. $Na_v1.5$ activity promotes motility and invasive behavior through several mechanisms, including MAPK activation [54, 55], up-regulation of CD44 expression [46], and

potentiation of Na^+/H^+ exchanger type 1 (NHE1) activity leading to cysteine cathepsin activation [56-58]. $Na_v1.5$ also promotes acquisition of an elongate mesenchymal-like phenotype, cortactin phosphorylation and cytoskeletal reorganization [46, 57]. Taken together, these data point to an important role for both $Na_v1.5$ and V_m in regulating morphological changes and migration. An important question is, therefore, how migratory behavior is regulated by electrical changes and Na^+ flux at the plasma membrane.

Here, we investigated the role of $Na_v1.5$ in regulating V_m in non-excitable breast cancer cells. We report that $Na_v1.5$ promotes steady state V_m depolarization, which in turn leads to localized activation of Rac1 at the plasma membrane, promoting morphological changes and migration. This work uncovers a novel and unexpected voltage-dependent mechanism for Rac1 activation, which would fine tune cell migration in response to ionic and/or electric field changes in the local microenvironment.

Materials and Methods

Chemicals

Iberiotoxin (IbTx), NS-1619, tetrodotoxin (TTX) and veratridine were purchased from Alomone Labs. Phenytoin was from Sigma. Ionomycin was from Cayman Chemical. EHT1864 was from Santa Cruz Biotechnology. Drugs were reconstituted as stock solutions according to manufacturer guidelines and diluted directly into culture medium and/or recording solutions at the indicated working concentrations.

Cell culture

MDA-MB-231 human breast cancer cells were cultured at 37°C, 5 % CO_2 in Dulbecco's modified eagle medium (DMEM) supplemented with 5% fetal bovine serum (FBS) and 4 mM

L-glutamine. MDA-MB-231 cells are a well-established cell line for examining the functional activity of $Na_v1.5$ in regulating cell behavior and they demonstrate robust endogenous expression of this channel [48-50, 53, 57-59]. Cells were confirmed to be mycoplasma-free by 4',6-diamidino-2-phenylindole (DAPI) staining method [60]. Molecular identity was confirmed by short tandem repeat analysis [61].

RNA interference

A GFP-expressing MDA-MB-231 cell line lacking functional $Na_v1.5$ expression was produced previously by lentiviral transduction of recombinant lentivirus for shRNA targeting $Na_v1.5$ (MISSION pLKO.1-puro shRNA transduction particles; Sigma) [46]. $Na_v1.5$-shRNA cells and cells non-targeting shControl cells were maintained in G418 (4 µl/ml, Sigma), blasticidin (2 µl/ml, AppliChem) and puromycin (0.1 µl/ml, Sigma).

Whole-cell patch clamp recording

The whole-cell patch clamp technique was used to record membrane current and voltage from cells grown on glass coverslips for 48-72 h. Voltage- and current-clamp recordings were made using a Multiclamp 700B amplifier (Molecular Devices) at room temperature. Membrane currents and V_m were digitized using a Digidata 1440A interface (Molecular Devices), low-pass filtered at 10 kHz and analyzed using pCLAMP 10.4 software (Molecular Devices). In voltage-clamp mode, signals were sampled at 50 kHz, and the series resistance was compensated by 40-60 %. Linear components of leak were subtracted using a P/6 protocol [62]. The standard extracellular physiological saline solution (PSS) contained the following components (in mM): 144 NaCl, 5.4 KCl, 1 $MgCl_2$, 2.5 $CaCl_2$, 5 HEPES and 5.6 glucose adjusted to pH 7.2 with NaOH. For the Na^+-free PSS, NaCl was replaced with 144 mM N-methyl-D-glucamine (NMDG) or choline chloride (ChoCl) adjusted to pH 7.2 with HCl. The standard intracellular (pipette) solution contained (in mM) 5 NaCl, 145 KCl, 2 $MgCl_2$, 1

$CaCl_2$, 10 HEPES and 11 EGTA adjusted to pH 7.4 with KOH. Free Ca^{2+} concentration in the solution was calculated using MaxChelator software (Stanford University). Na^+ current was activated by depolarizing from -120 mV (250 ms) to voltages in the range -80 to +30 mV in 5 mV increments (50 ms).

Membrane potential recording

The steady-state V_m was recorded in I = 0 mode within 5 s of achieving the whole-cell configuration. To monitor the continuous V_m in individual cells in response to pharmacological treatments, cells were held in the whole-cell configuration for 6 min, with 60 s in the standard PSS, followed by 150 s in treatment and a further 150 s for washout of treatment. The mean V_m over the last 5 s in each of the three stages was used to compare the V_m data. The V_m signals were sampled at 200 Hz. Liquid junction potentials were calculated using the integrated tool in Clampex 10.4. Dose-response data were fitted to a sigmoidal logistic equation

$$\%\, block = \frac{100}{1 + (\frac{IC_{50}}{[Drug]})^n}$$

where IC_{50} is the concentration of drug at which half of its maximal effect occurs; and n is the slope giving the Hill coefficient.

Perforated patch clamp recordings

The perforated patch clamp technique was used to record $K_{Ca}1.1$ currents. The intracellular solution used in perforated patch recording contained (in mM) 5 choline-Cl, 145 KCl, 2 $MgCl_2$, 10 HEPES and 1 EGTA adjusted to pH 7.4 with KOH. Nystatin (150 μM) in DMSO was made up and added the perforated patch intracellular solution on the day of the experiment. Typical series resistance ranged between 20-40 MΩ. $K_{Ca}1.1$ current was elicited

by depolarizing from -120 mV (250 ms) to voltages in the range -60 to +90 mV in 10 mV increments (300 ms). The outward current data were fitted to a single exponential decay [63]

$$Y = Y_0 \times e^{kx}$$

where k is the rate constant.

Intracellular Na^+ and Ca^{2+} imaging

Measurement of $[Na^+]_i$ was performed as described in [64] with minor modifications. Briefly, 6×10^4 cells grown on glass coverslips for 24 h were labelled with 5 μM SBFI-AM (Sigma) and 0.1 % v/v Pluronic F-127 (Life Technologies) in DMEM with 0 % FBS at 37 °C in the dark for 1 h. Excess SBFI-AM was washed out with 37 °C DMEM supplemented with 5 % FBS. The coverslip was assembled into a RC-20H closed bath imaging chamber (Warner Instruments) and observed at room temperature using a Nikon Eclipse TE200 epifluorescence microscope at 40X. SBFI was alternately excited at 340 and 380 nm, and the fluorescence emission at 510 nm was collected at 8-bit depth using a Rolera-XR Fast 1394 CCD camera (QImaging) controlled by SimplePCI software (Hamamatsu). Calibration of $[Na^+]_i$ was performed after each recording by perfusing two solutions on the cells: 10 and 20 mM Na^+. They contained (in mM) 149.4 NaCl + KCl, 1 $MgCl_2$, 2.5 $CaCl_2$, 5 HEPES, 5.6 glucose and 0.02 gramicidin (Sigma), adjusted to pH 7.2 with KOH. In each experimental repeat, $[Na^+]_i$ of ≥ 7 individual cells in the field of view were calculated individually and then averaged. For Ca^{2+} imaging, cells were labelled with 1 μM Fura-2 AM (PromoKine) using the same procedure as above, with an additional wash step using 37 °C phenol red-free DMEM (Life Technologies) after 1 h incubation with the dye, and the images were captured at 20X. In each experimental repeat, the $[Ca^{2+}]_i$ of ≥ 17 individual cells in the field of view were measured. Each experiment was repeated at least three times.

Western blotting

Western blotting was performed as described previously [59]. The primary antibodies were: mouse anti-$K_{Ca}1.1$ (1:500; NeuroMab) and mouse anti-α-tubulin (1:10,000; Sigma).

Cell migration assay

Cell migration was measured using wound heal assays [53]. Label-free ptychographic microscopy was used to monitor motility in real time [65, 66]. Images were acquired over 16 h at 9 min intervals using a Phasefocus VL-21 microscope with an 10X (0.25 NA) lens using 640 nm illumination and equipped with an environmental chamber maintaining the cells at 37 °C in 5% CO_2. The wound healing experiment was repeated three times on separate days. Image sequences of gap closure were processed using Phasefocus Cell Analysis Toolbox (CAT) software in order to segment and track individual cells at the leading edge and measure wound area. For each image sequence, the following parameters were automatically measured: change in normalized gap area over time; $t_{1/2}$ for gap closure (h), determined by applying a linear fit to the normalized wound area reduction from t = 0 until the time at which the area reduces by 50 %; collective migration (μm/h), defined as:

$$V_{migration} = \frac{|slope|}{2 \times l}$$

where slope is the rate of area of scratch closure and l is the length of the scratch; instantaneous velocity per cell (μm/s), considering segmented cells with track lengths of ≥ 5 frames; and directionality of leading edge cells tracked for ≥ 5 frames, relative to the center of the scratch.

Cell proliferation and invasion assays

Cell proliferation was measured using the thiazolyl blue tetrazolium bromide (MTT) assay, as described [53]. Cell invasion was quantified using 24-well Corning BioCoat Matrigel Invasion Chambers according to the manufacturer's guidelines. Briefly, 2.5×10^4 MDA-MB-231 cells

were seeded in the upper compartment supplemented with 1 % FBS and appropriate treatments. The lower compartment contained 10 % FBS and appropriate treatments. Cells were incubated at 37 °C for 24 h before the removal of non-invaded cells from the upper chamber using cotton buds. Cells that had invaded through the polyethylene terephthalate membrane were fixed using 4 % paraformaldehyde for 10 min and were washed three times with phosphate buffered saline (PBS), 5 min/time, before staining with DAPI. The membrane was then mounted on a glass microscope slide. DAPI-positive cells on the membrane were viewed at 20X using a Nikon Eclipse TE200 epifluorescence microscope. Experiments were performed on duplicate wells and repeated ≥ 3 times.

Immunocytochemistry

Cells (1.6×10^5) were cultured on glass coverslips in 4-well plates for 48 h in order to form confluent monolayers. Wounds were made on the coverslip using a P200 pipette tip and debris was washed off with 37 °C DMEM. Appropriate treatments were subsequently applied, and cells were allowed to migrate into the wound for 3 h. Cells were fixed in 4 % paraformaldehyde for 10 min and immunocytochemistry was performed, as described [59]. The following primary antibodies were used: rabbit anti-$Na_v1.5$ (1:100; Alomone); rabbit anti-$K_{Ca}1.1$ (1:100; Neuromab); mouse anti-Rac1-GTP (1:500; NewEast Biosciences); rabbit anti-total Rac1 (1:10; NewEast Biosciences); mouse anti-CD44 (1:100; AbD Serotec). The secondary antibodies were Alexa 488 or 568-conjugated goat anti-mouse and Alexa 488 or 568-conjugated goat anti-rabbit (1:500; Life Technologies). In some experiments, cells were counter-stained with Alexa 633-conjugated phalloidin (1:50; Life Technologies). In experiments where permeabilized cells were labelled with Alexa 568-conjugated annexin V (1:20; Life Technologies), primary and secondary antibodies were incubated in Ca^{2+}-containing annexin V binding buffer (Life Technologies) to preserve annexin V binding. Coverslips were then mounted on glass microscope slides using Prolong Gold with DAPI (Life Technologies). The slides were examined using a Zeiss LSM 710 confocal microscope

at 40X. Images (512 x 512 or 1024 x 1024 pixels, dependent on experiment) were initially processed with the Zeiss Zen 2 software, and later exported into ImageJ for analysis. Brightness/contrast was adjusted using the ImageJ “Auto” function.

Morphology and lamellipodium scoring

Circularity was calculated on manually segmented cells using the free-hand tool in ImageJ [67]:

$$Circularity = 4\pi \times \frac{Area}{Perimeter^2}$$

Values approaching 0 indicate a more elongated cell morphology. Feret’s diameter was measured as the maximum distance between any two points along the cell boundary. Three experimental repeats were performed, and 20-25 cells per condition were analyzed for every repeat. To score lamellipodia formation, cells were categorized into two groups: with and without lamellipodium. For each of the three experimental repeats, 40-50 cells per condition were analyzed blinded to treatment.

Analysis of Rac1 localization in the lamellipodium

The signal densities of F-actin, Rac1-GTP and total Rac1 in the lamellipodium were analyzed in arcs at various distances from the leading edge as described [68]. The ImageJ Radial Profile Extended plugin (Philippe Carl, CNRS, France) was used with starting radius = 0.43 μm, radius increment = 0.43 μm, ending radius = 5.6 μm and total integrated angle = 90°, resulting in 13 arcs in total. Signal densities on each of the arcs were obtained and were normalized to those on the innermost arc. Typically, 20-30 cells at the edge of the wound were analyzed for each condition and the experiment was repeated three times.

Colocalization analysis

Colocalization of annexin V and Rac1-GTP labeling within regions of interest drawn around the lamellipodium was evaluated using the Coloc2 plugin in ImageJ. The approximate point spread function on acquired images of 1024 x 1024 pixels was 2.71 pixels. For each region of interest, the thresholded Manders M1 and M2 coefficients for annexin V and Rac1-GTP were computed [69], together with the Li's intensity correlation coefficient [70]. Measurements were taken from 30 cells per condition over three experimental repeats.

In vitro Rac1 activity assay

Cells were cultured to 70 % confluency in 6-well plates prior to addition of pharmacological treatment(s). After incubation for 24 h, total cellular Rac1 activity was evaluated in cell lysates using a colorimetric ELISA-based small GTPase activation assay, according to the manufacturer's instructions (G-LISA; Cytoskeleton, Inc) [71]. Measurements were obtained from duplicate wells and the experiment was repeated three times.

Live cell imaging of Rac1 biosensor activation

Cells (1.6×10^5) were cultured in 8-well chamber glass slides. After incubation for 24 h, cells were transfected with 200 ng of a biosensor for Rac1 activation (pTriEx4-Rac1-2G; Addgene plasmid # 66110) [72] using Fugene (Roche) [59]. 48 h following transfection, appropriate treatments in phenol red-free DMEM were applied for 3 h prior to imaging. FRET imaging of biosensor activation was performed at room temperature using a Nikon Eclipse TE200 epifluorescence microscope with a 40X (NA 0.60) objective. Acquisition from cells expressing low levels of the biosensor was performed at 8-bit depth using a Rolera-XR Fast 1394 CCD camera (QImaging) controlled by SimplePCI software (Hamamatsu). Acquisition time for donor and FRET channels was typically 200 ms. The donor and acceptor channels were acquired sequentially. The donor, monomeric teal fluorescent protein (mTFP), was

excited at 436 nm and emission was collected at 480 nm. FRET emission was collected above 540 nm. The acceptor (Venus) was excited at 480 nm and emission collected above 540 nm. Visualization of cells transfected with a control plasmid expressing mTFP alone, created by site-directed mutagenesis [59], revealed minimal bleed-through in the FRET and Venus channels. Images were taken from ≥49 cells across three experimental repeats. Image processing was performed using ImageJ. Cells were manually segmented using the distribution of biosensor (donor mTFP signal). Images were then background subtracted prior to calculation of the FRET/mTFP integrated density ratio for each cell.

Statistics

Data are presented as mean ± SEM. GraphPad Prism 7.0d was used to perform all statistical analyses. Polar histograms were plotted using OriginLab Origin 2017. For normally distributed data, paired or unpaired Student's two-tailed t-test was used to compare two groups, as appropriate. Multiple comparisons were made using 1-way ANOVA or repeated measures ANOVA followed by Tukey *post-hoc* tests, as appropriate. For repeated measures data that were not normally distributed, Friedman test with Dunn's *post-hoc* tests were used. Fisher's exact test was used to examine the distribution of samples within a population. Contingency table data were analyzed using χ^2 test. Colocalization data were analyzed by 2-way ANOVA. Results were considered significant at $P < 0.05$.

Results

$Na_v1.5$ channels depolarize the membrane potential of breast carcinoma cells

The V_m of motile cancer cells is generally more depolarized than in terminally-differentiated non-cancer cells [21]. In addition, both depolarized V_m and $Na_v1.5$ channel activity correlate

with metastatic potential [49]. However, it is not known whether the relationship between $Na_v1.5$, V_m and cell behavior is causal. Here, we first investigated whether Na^+ conductance through plasma membrane $Na_v1.5$ channels contributes to the depolarized V_m that has been reported previously in MDA-MB-231 cells [49]. $Na_v1.5$ carries a persistent inward Na^+ current, small in amplitude compared to the transient Na^+ current, which plays an important role in shaping the action potential firing pattern, especially in the subthreshold voltage range [73]. In non-excitable cells, this would allow significant accumulation of Na^+ over an extended period, potentially permitting V_m depolarization at steady state. $Na_v1.5$ is robustly expressed in MDA-MB-231 cells, both in intracellular compartments and at the plasma membrane (Figure 1A) [49, 53, 57, 58]. We measured Na^+ currents carried by $Na_v1.5$ using whole-cell voltage clamp recording. Depolarization from -120 mV to -10 mV elicited both transient and persistent inward Na^+ currents (Figure 1B, C). Analysis of the voltage-dependent activation and steady-state inactivation of the Na^+ current revealed a window current between -50 mV and -10 mV (Figure 1D, E). We next investigated whether $Na_v1.5$ could regulate the V_m. Stable suppression of $Na_v1.5$ expression using lentiviral shRNA [46] significantly hyperpolarized the V_m, measured using whole-cell current clamp recording, from -12.6 ± 0.9 mV to -16.0 ± 0.8 mV compared to control cells ($P < 0.01$; $n = 16$; t test; Figure 1F). Thus, $Na_v1.5$ is required to depolarize the steady-state V_m.

We next evaluated the effect of pharmacologically perturbing $Na_v1.5$ activity. The specific VGSC blocker TTX (30 μM) reversibly inhibited the transient and persistent Na^+ current ($P < 0.001$ and $P < 0.05$, respectively; $n \geq 5$; repeated measures ANOVA with Tukey test; Figure 2A-D), consistent with previous reports [48-50]. TTX also significantly hyperpolarized the V_m from -13.2 ± 1.3 mV to -17.5 ± 1.6 mV ($P < 0.01$; $n = 17$; repeated measures ANOVA with Tukey test; Figure 2E, F). On the other hand, the carrier for TTX (148 μM sodium citrate, pH = 4.8) had no effect on the V_m (Figure S1A, B). In agreement with the TTX data, the VGSC-inhibiting antiepileptic drug, phenytoin (100 μM) also significantly reduced the transient and persistent Na^+ current and hyperpolarized the V_m (Figure S1C-K). In contrast, veratridine

(100 μM), which increases channel open probability by inhibiting inactivation [74], increased the persistent Na^+ current (Figure 2G, H and Figure S2A, B) and depolarized the V_m from -16.37 ± 1.4 mV to -12.6 ± 1.3 mV ($P < 0.05$; n = 13; t test; Figure 2H). In summary, these data show that pharmacological or genetic inhibition of $Na_v1.5$ hyperpolarizes the steady-state V_m, whereas increasing the persistent Na^+ current depolarizes the V_m. Thus, persistent current carried by $Na_v1.5$ contributes to V_m depolarization.

Membrane potential depolarization is dependent on extracellular Na^+

To evaluate the sufficiency of extracellular Na^+ to determine the V_m, we next removed Na^+ in the extracellular solution during recording. Replacement of extracellular NaCl with choline chloride reversibly hyperpolarized the V_m from -10.4 ± 1.0 to -20.4 ± 2.0 mV ($P < 0.001$; n = 10; repeated measures ANOVA with Tukey test; Figure 3A, B). Using NMDG to replace extracellular Na^+ had a similar hyperpolarizing effect (Figure S2C, D). Thus, extracellular Na^+ is required for steady-state V_m depolarization.

Inward Na^+ current through $Na_v1.5$ channels would be expected to elevate the intracellular Na^+ level ($[Na^+]_i$) at steady state. Indeed, VGSCs have previously been shown to increase $[Na^+]_i$ [64, 75]. We therefore next investigated the involvement of extracellular Na^+ in setting $[Na^+]_i$ using the ratiometric Na^+ indicator SBFI-AM (Figure 3C, D). Replacement of extracellular Na^+ with NMDG significantly reduced the steady-state $[Na^+]_i$ from 15.6 ± 1.7 mM to 7.6 ± 2.9 mM ($P < 0.001$; n = 3; ANOVA with Tukey test; Figure 3E). Treatment with TTX also significantly reduced the steady-state $[Na^+]_i$, suggesting that $Na_v1.5$ activity contributes to this elevation of $[Na^+]_i$ ($P < 0.05$; n ≥ 10; ANOVA with Tukey test; Figure 3E). In agreement with this, the $[Na^+]_i$ of $Na_v1.5$-shRNA cells was significantly lower than for control cells (9.4 ± 1.2 mM *vs.*13.5 ± 0.6 mM; $P < 0.01$; n = 3; t test; Figure 3F). On the other hand, $Na_v1.5$ inhibition with TTX had no effect on $[Ca^{2+}]_i$ (Figure S3A-D). Together, these data suggest that Na^+ influx through $Na_v1.5$ channels increases $[Na^+]_i$, but not $[Ca^{2+}]_i$.

K_{Ca}1.1 regulates the membrane potential but not the Na^+ level

Na_v1.5 channels enhance cell migration, invasion, tumor growth and metastasis [46, 49, 50]. Given that Na_v1.5 depolarizes the steady-state V_m, and that V_m depolarization is functionally instructive in regulating cellular behavior [21], we reasoned that Na_v1.5 may regulate cell migration via setting the V_m. Thus, we sought a means by which to manipulate the V_m independent of Na_v1.5 in order to separate the effects of V_m and $[Na^+]_i$ on downstream signaling. To do this, we took advantage of ubiquitously expressed large conductance Ca^{2+}-activated K^+ channel, K_{Ca}1.1 [76]. We verified that K_{Ca}1.1 was robustly expressed in MDA-MB-231 cells [77-79], and its expression was unaffected by Na_v1.5 downregulation (Figure 4A, B). Next, using the perforated patch clamp mode in order to maintain endogenous $[Ca^{2+}]_i$, we found that the K_{Ca}1.1 opener NS-1619 (1 μM) [80] increased outward K^+ current, confirming K_{Ca}1.1 activity (Figure 4C, D). Co-application of the K_{Ca}1.1 channel blocker iberiotoxin (100 nM) inhibited the potentiating effect of NS-1619 on the outward current (Figure 4C, D), confirming specificity of NS-1619. We next studied the effect of NS-1619 on the V_m. NS-1619 hyperpolarized the steady-state V_m in a dose-dependent manner (Figure 4E). Importantly, 1 μM NS-1619 hyperpolarized the V_m by 4.4 mV from -10.6 ± 1.3 mV to -15.0 ± 0.6 mV ($P < 0.01$; $n \geq 12$; t test; Figure 4F). This shift is equivalent to the hyperpolarization elicited by inhibiting Na_v1.5 activity (Figure 2F, I). In contrast, NS-1619 treatment did not significantly alter the $[Na^+]_i$ ($P = 0.93$; $n = 22$; paired t test; Figure 4G) or $[Ca^{2+}]_i$ (Figure S3E, F). Finally, the V_m recorded using the standard intracellular solution (free $[Ca^{2+}] = 5.7$ nM) was not significantly different from that recorded using intracellular solution with 100 nM free $[Ca^{2+}]$ ($P = 0.82$; $n = 12$; t-test; Figure 4H), suggesting that at physiological $[Ca^{2+}]_i$ [81, 82], K_{Ca}1.1 channels do not contribute to regulating the V_m in the absence of NS-1619. In summary, activation of K_{Ca}1.1 hyperpolarizes the V_m to the same extent as Na_v1.5 inhibition, thus providing an experimental means by which to manipulate the V_m independent of Na^+.

Na_v1.5-dependent membrane potential depolarization regulates cell migration and morphology

Using NS-1619 and TTX as tools to modify the V_m independent of, or as a result of Na_v1.5 activity, respectively, we next investigated the effect of V_m depolarization on cell migration in wound healing assays using label-free ptychographic imaging (Figure 5A). Both TTX and NS-1619 slowed the rate of wound closure (Figure 5B). The $t_{1/2}$ of wound closure increased from 5.7 ± 1.1 h to 9.8 ± 0.7 h in the presence of TTX and 9.9 ± 0.1 h in the presence of NS-1619 ($P < 0.05$; $n \geq 5$; ANOVA with Tukey test; Figure 5C). Similarly, the collective migration of cells moving into the wound was reduced from 7.8 ± 0.7 μm/h to 5.5 ± 0.4 μm/h in the presence of TTX and 4.9 ± 0.5 μm/h in the presence of NS-1619 ($P < 0.05$; $n \geq 5$; ANOVA with Tukey test; Figure 5D). The instantaneous velocity of individual cells at the leading edge was also reduced from $6.2 \times 10^{-3} \pm 5.6 \times 10^{-5}$ μm/s to $4.7 \times 10^{-3} \pm 5.0 \times 10^{-5}$ μm/s and $4.4 \times 10^{-3} \pm 4.5 \times 10^{-5}$ μm/s, for TTX- and NS-1619-treated cells, respectively ($P < 0.001$; $n \geq 2662$; Kruskal-Wallis with Dunn's test; Figure 5E). In addition, both TTX and NS-1619 caused a small, but statistically significant, disruption in the directionality of cells at the leading edge, reducing the proportion of cells migrating directly into the wound ($P < 0.001$; Friedman with Dunn's test; Figure 5F). Hyperpolarizing the V_m with NS-1619 did not significantly alter cell proliferation measured in an MTT assay (Figure S4A). Given that inhibiting Na_v1.5 with TTX has no effect on the proliferation of MDA-MB-231 cells [49, 50, 56], together, these data suggest that both Na_v1.5 activity and V_m depolarization promote cellular migration, without affecting proliferation. On the other hand, whilst TTX significantly reduced invasion into Matrigel, consistent with previous reports [46, 48-50, 53, 83], NS-1619 had no effect (Figure S4B, C). Thus, Na_v1.5 promotes cellular migration, but not invasion, via V_m depolarization.

Na_v1.5 promotes an elongate, mesenchymal-like motile morphology [46, 57, 83]. This morphological modulation has been shown to occur through two potentially overlapping

mechanisms: (1) regulation of adhesion-mediated signaling *via* β1 subunits and up-regulation of CD44 expression [46, 59], and (2) *via* increased Src kinase activity, phosphorylation of the actin-nucleation-promoting factor cortactin, and F-actin polymerization [57]. In addition, the V_m has been shown to promote reorganization of the actin filament network and cytoskeleton in other cell types [26-30]. However, the potential involvement of V_m in $Na_v1.5$-mediated signaling is not known. We thus investigated the participation of $Na_v1.5$-mediated V_m depolarization in regulating cell morphology. TTX (30 μM) significantly increased cell circularity after 3 h ($P < 0.001$; $n \geq 61$; ANOVA with Tukey test; Figure 6A, B), consistent with previously published data [57]. NS-1619 (1 μM) also increased circularity ($P < 0.05$; $n \geq 61$; ANOVA with Tukey test; Figure 6A, B). Similarly, both TTX and NS-1619 significantly reduced the Feret's diameter (maximum caliper distance across the cell; $P < 0.01$; $n \geq 57$; ANOVA with Tukey test; Figure 6C). These data suggest that both $Na_v1.5$ activity and V_m depolarization promote acquisition of an elongate phenotype.

Given that $Na_v1.5$-mediated V_m depolarization promotes both morphological changes and cellular migration, we postulated that it might regulate formation of lamellipodia in migrating cells. We therefore scored the number of migrating cells with visible lamellipodia in a wound healing assay following treatment with TTX and NS-1619. Both treatments significantly reduced the proportion of cells with a lamellipodium in the measured population ($P < 0.001$; $n \geq 139$ cells per condition; χ^2 test; Figure 6D). Together, these findings suggest that $Na_v1.5$-mediated V_m depolarization promotes a change in cellular morphology towards an elongate phenotype, and increases lamellipodia formation, thus potentiating cellular migration.

$Na_v1.5$-dependent membrane potential depolarization regulates Rac1 activation

The small GTPase Rac1, together with Rho and cdc42, plays a critical role in regulating cytoskeletal organization and cell motility [84]. In addition, Rac1 also regulates the formation of lamellipodia, cell motility and the directionality of cell movement [5]. We therefore postulated that $Na_v1.5$ and V_m depolarization may regulate the level of active (GTP-bound) Rac1 in the lamellipodia of migrating cells. We treated migrating cells with NS-1619 and TTX for 3 h and then evaluated distribution of Rac1-GTP by quantifying immunocytochemical signal density across concentric arcs in the lamellipodium of individual cells (Figure 7A, B). As reported previously, a large quantity of Rac1 is present intracellularly in the perinuclear region, although there is also an enrichment of Rac1-GTP in the lamellipodium, consistent with its critical role in this region [5, 7]. Both TTX and NS-1619 significantly reduced the peak Rac1-GTP signal at the leading edge of migrating cells ($P < 0.05$; $n \geq 66$; 1-way ANOVA with Tukey test; Figure 7C). However, the level of total cellular Rac1-GTP, determined in whole cell lysates, was unaffected by TTX treatment ($P = 0.80$; $n = 6$; t test; Figure 7D). Given that the majority of Rac1 is present intracellularly (Figure 7A) [8, 85], these data suggest that $Na_v1.5$ may regulate Rac1 locally at the plasma membrane and/or within lamellipodia. We next evaluated the effect of TTX and NS-1619 on distribution of Rac1-GTP *vs.* total Rac1 using an antibody that does not distinguish between GDP- and GTP-bound forms of Rac1 (Figure 7E). The peak total Rac1 signal at the leading edge of migrating cells was unaffected by both TTX and NS-1619 ($P = 0.69$; $n \geq 60$; 1-way ANOVA; Figure 7F, G). Thus, the ratio of peak Rac1-GTP to total Rac1 at the leading edge was significantly reduced by both TTX and NS-1619 ($P < 0.001$; $n = 3$; 1-way ANOVA; Figure 7G). These data suggest that V_m depolarization caused by steady state $Na_v1.5$ activity increases Rac1 activation at the leading edge of migrating cells.

V_m depolarization promotes clustering and activation of the small GTPase K-Ras as a result of voltage-dependent redistribution of charged phospholipids including phosphatidylserine [24]. Given that Rac1 is also anchored to the inner leaflet of the plasma membrane via interaction with phosphatidylserine [10, 86], we reasoned that a similar voltage-dependent

mechanism may be responsible for Rac1 activation in the lamellipodia. We therefore next evaluated the effect of V_m depolarization on colocalization of Rac1-GTP with phosphatidylserine, using annexin V as a marker (Figure 8A). Treatment of migrating cells with TTX and NS-1619 reduced colocalization of Rac1-GTP with phosphatidylserine in the lamellipodia (Figure 8B-D). This was confirmed by quantification of thresholded Manders colocalization coefficients for phosphatidylserine and Rac1-GTP ($P < 0.01$; $n = 30$; 2-way ANOVA with Tukey test; Figure 8E). Similarly, the TTX and NS-1619 treatments both reduced the Li's intensity correlation quotient ($P < 0.001$; $n = 30$; 1-way ANOVA with Tukey test; Figure 8F). These data support the notion that V_m depolarization increases Rac1 localization in the lamellipodia as a result of its interaction with phosphatidylserine.

In order to evaluate whether $Na_v1.5$-mediated V_m depolarization promotes Rac1 activity in live cells, we next employed a genetically encoded Rac1 FRET biosensor to monitor Rac1 activation. In agreement with previous reports [72], the biosensor showed a general gradient of Rac1 activation increasing from the cell interior towards the periphery, consistent with its critical role in actin remodeling at the edge of migrating cells (Figure 9A) [5]. Treatment with TTX did not affect biosensor distribution (Figure 9A), but suppressed activation at the periphery (Figure 9B, C). Quantification of FRET across the whole cell revealed that TTX significantly reduced Rac1 activation to 48.6 ± 5.2 % of control ($P < 0.001$; $n \geq 49$; t test; Figure 9D). Together, these results indicate that blockade of $Na_v1.5$ channels suppresses Rac1 activation at the cell periphery.

$Na_v1.5$-mediated morphological changes are dependent on Rac1 activation

Given that $Na_v1.5$-dependent V_m depolarization promotes morphological changes leading to increased cell migration (Figures 5, 6), and that $Na_v1.5$ promotes activation of Rac1 (Figures 7, 8, 9), which in turn, plays a key role in regulating cellular morphology and migration [5], we analyzed the impact of Rac1 inhibition on $Na_v1.5$-dependent changes in cell morphology

(Figure 10A). The specific Rac1 inhibitor EHT1864 increased circularity and reduced Feret's diameter in a dose-dependent manner (Figure S5A, B). Furthermore, EHT1864 increased circularity to a similar extent to TTX ($P < 0.001$; $n \geq 308$; 1-way ANOVA with Tukey test; Figure 10B, C). Importantly, co-application of EHT1864 with TTX had no additive effect on circularity or Feret's diameter (Figure 10B, C). These results show that Rac1 activity is required to transduce the $Na_v1.5$-dependent V_m depolarizing signal in order to promote acquisition of an elongate, motile cell phenotype (Figure 10D).

Discussion

Here we identify $Na_v1.5$-mediated V_m depolarization as a regulator of Rac1 activation. Thus, we link ionic and electrical signaling at the plasma membrane to small GTPase-dependent cytoskeletal reorganization and cellular migration. We show that depletion of extracellular Na^+ or blockage of $Na_v1.5$ channels reversibly hyperpolarizes the V_m at the timescale of minutes. We further show that $Na_v1.5$-dependent V_m depolarization increases Rac1 colocalization with phosphatidylserine at the leading edge of migrating cells, promoting Rac1 activation, and resulting in acquisition of a motile, mesenchymal-like cellular phenotype. We therefore propose that $Na_v1.5$ may serve as a sensor for local changes in the ionic microenvironment, thus permitting voltage-dependent activation of Rac1 to fine tune cell migration.

Ion conductance, membrane potential and migration

We show that $Na_v1.5$ carries a persistent inward Na^+ current in MDA-MB-231 cells. In agreement with the work of others, we report incomplete inactivation of $Na_v1.5$ resulting in a small voltage window encompassing the V_m, thus supporting this persistent Na^+ current [46, 50, 53, 56, 58, 87]. The persistent inward Na^+ current carried by $Na_v1.5$ contributes to steady-state V_m depolarization. Our findings agree with another study in H460 non-small cell

lung cancer cells, in which $Na_v1.7$ channels were shown to depolarize the V_m by ~10 mV [75]. In addition, it has previously been shown that VGSCs contribute to steady-state V_m depolarization and viability in rat optic nerve axons and spinal cord astrocytes over a time course of hours [88, 89], suggesting that this mechanism persists over an extended period. There may be other Na^+-permeable pathway(s) also contributing to V_m regulation in non-excitable cells, e.g. via epithelial Na^+ channels [90], Na^+-K^+ ATPase [81], and NHE1 [58]. In addition, the V_m may also be dependent on the activity of transporters and channels regulating the movement of other ions, including Cl^- and K^+ [21]. The depolarized resting V_m reported here may therefore be attributed not only to the high permeability to Na^+ but also to the low expression/activity of hyperpolarizing K^+ channels.

Relatively small alterations in V_m can be functionally significant. For example, during synaptic transfer from photoreceptors to ganglion cells in turtle retina, V_m depolarizations as small as 5 mV are sufficient to activate paired ganglion cells [91]. The V_m can function as an instructive signal to regulate cell cycle progression in proliferating cells [24, 36, 92, 93]. V_m depolarization can regulate other cellular behaviors, including differentiation [25] and cytoskeletal reorganization [26-30]. At the tissue level, changes in V_m can also regulate morphogenesis, regeneration and tumorigenesis [31-37]. Several studies have shown that epithelial cells undergo V_m depolarization when migrating into wounds [26, 27]. However, an interesting and novel finding of our study here is that V_m depolarization is not simply a consequence of motile behavior [18], but is *itself* a master regulator of morphological changes and migration. Here, we found that hyperpolarizing the V_m by ~5 mV reduced migration by ~30 %. The fact that this level of V_m hyperpolarization did not completely inhibit migration raises the possibility that additional hyperpolarization may have a further inhibitory effect. This would suggest that other ion conductance routes contributing to the V_m may also be involved in migration regulation. Nonetheless, our data underscore that persistent Na^+ influx through $Na_v1.5$ channels leads to V_m depolarization, which in turn promotes cell migration.

Given the general trend towards depolarized V_m both in cancer cells [21, 36, 49], and in epithelial cells undergoing migration [26, 27], we propose that voltage-dependent migratory behavior may be a general cellular phenomenon. For example, although involvement of V_m was not directly investigated, activation of the V_m-hyperpolarizing channel $K_{Ca}1.1$ with NS-1619 reduces migration of glioma cells [94]. Furthermore, VGSCs have been detected in cells from a broad range of tumor types, where they potentiate migration and invasion [51, 52]. We therefore argue that the results presented here have broad applicability to other cell types.

Voltage-dependent regulation of Rac1 activation

V_m depolarization promotes K-Ras clustering and subsequent activation [24]. Various small GTPases, including K-Ras and the Rho GTPases, are anchored to the inner leaflet of the plasma membrane through interaction with the anionic phospholipids PIP2, PIP3 and phosphatidylserine [10-12, 24, 86]. In the case of K-Ras, clustering and activation has been shown to arise as a result of depolarization-induced redistribution of phosphatidylserine and PIP2 in the inner leaflet of the phospholipid bilayer, to which the K-Ras is anchored [24]. Our major discovery here is that Rac1 activation is also voltage-dependent. Our data show that $Na_v1.5$-mediated V_m depolarization causes Rac1 activation, likely as a result of voltage-dependent redistribution of phosphatidylserine (Figure 10D). Thus, V_m-dependent signaling is not exclusively limited to mitogenic cascades but is also a key regulator of morphological changes and migration.

A growing body of evidence implicates V_m depolarization in regulation of small GTPase activity. For example, V_m has been shown to regulate the activity of GEF-H1, which, in turn, regulates the activity of the Rho/Rho kinase pathway [95]. V_m depolarization-dependent activation of Rho and subsequent cytoskeletal organization has been shown to be Ca^{2+}-

independent [30]. In agreement with this, our data also imply that Ca^{2+} is not involved as a signaling intermediary in V_m depolarization-induced Rac1-mediated promotion of migration. On the other hand, in ATP-stimulated microglia, VGSC activity increases $[Ca^{2+}]_i$, and activates ERK and Rac1, promoting migration [96]. V_m depolarization-induced activation of Ras and Rap1 has also been reported in mouse cortical neurons [97].

The mechanism uncovered here may feed into, and interact with, additional signaling pathways which have been shown to be dependent on $Na_v1.5$ activity. For example, $Na_v1.5$ has been shown to promote Src kinase activity and phosphorylation of cortactin and cofilin [57]. Thus, $Na_v1.5$-induced V_m depolarization may activate Rac1, increasing cortactin phosphorylation and therefore enhancing cofilin activity and actin filament polymerization. Src has also been shown to regulate Rac1 activity, suggesting the potential for feedback regulation [98]. $Na_v1.5$ positively regulates the expression of the metastasis-promoting protein CD44, which may activate Src and therefore contribute to this process [46, 54, 55, 99, 100]. In addition, $Na_v1.5$ is expressed on astrocytes where it regulates migration by promoting reverse Na^+/Ca^{2+} exchange [101, 102]. Furthermore, $Na_v1.5$ is expressed on the endosome of macrophages, where it regulates endosomal acidification [103]. On the other hand, $Na_v1.6$ is expressed within macrophage podosomes, where it promotes invasion via intracellular Na^+ release [104]. $Na_v1.5$ and $Na_v1.6$ are also expressed on microglia, where the latter has been shown to also regulate migration and cytokine release [105]. Together, these studies suggest that VGSCs may further regulate the behavior of non-excitable cells via pathways in addition to the one identified here.

Implications for our understanding of metastasis

We provide evidence that $Na_v1.5$ contributes to steady-state V_m depolarization, which in turn promotes V_m-dependent Rac1 activation, lamellipodial protrusion formation and cellular migration. These data are in agreement with the previously reported role for VGSCs in

regulating morphology and migration of tumor cells [45, 48, 49, 57, 106, 107]. It is therefore conceivable that depolarization-dependent Rac1 activation may contribute to metastatic dissemination in response to local ionic changes in the tumor microenvironment. Thus, pharmacological targeting of VGSCs, which inhibits metastasis in preclinical models [45, 83, 108], may provide therapeutic benefit via V_m hyperpolarization and downregulation of V_m-dependent small GTPase activation. In conclusion, our results reveal a new role for $Na_v1.5$ channels as voltage-dependent activators of Rac1 signaling to promote cellular migration.

Statement of Ethics

The authors have no ethical conflicts to disclose.

Disclosure Statement

The authors have no conflicts of interest to declare.

Funding Sources

This work was supported by the Medical Research Council [G1000508], Cancer Research UK [A25922] and a Radhika V Sreedhar Scholarship. The authors declare no competing financial interests.

Author contributions

MY and WB contributed to the conception and design of the work. MY, AJ, RK, RS, PO'T and WB contributed to acquisition, analysis, and interpretation of data for the work. MY, RK, RS, PO'T and WB contributed to drafting the work and revising it critically for important intellectual content. All authors approved the final version of the manuscript.

References

1 Bravo-Cordero JJ, Hodgson L, Condeelis J: Directed Cell Invasion and Migration During Metastasis. Curr Opin Cell Biol 2012;24:277-283.
2 Friedl P, Locker J, Sahai E, Segall JE: Classifying collective cancer cell invasion. Nat Cell Biol 2012;14:777-783.
3 Krause M, Gautreau A: Steering cell migration: lamellipodium dynamics and the regulation of directional persistence. Nat Rev Mol Cell Biol 2014;15:577-590.
4 Ridley AJ: Rho GTPase signalling in cell migration. Curr Opin Cell Biol 2015;36:103-112.
5 Wu YI, Frey D, Lungu OI, Jaehrig A, Schlichting I, Kuhlman B, Hahn KM: A genetically encoded photoactivatable Rac controls the motility of living cells. Nature 2009;461:104-108.
6 Marei H, Malliri A: GEFs: Dual regulation of Rac1 signaling. Small GTPases 2017;8:90-99.
7 Garcia-Mata R, Boulter E, Burridge K: The 'invisible hand': regulation of RHO GTPases by RHOGDIs. Nat Rev Mol Cell Biol 2011;12:493-504.
8 Das S, Yin T, Yang Q, Zhang J, Wu YI, Yu J: Single-molecule tracking of small GTPase Rac1 uncovers spatial regulation of membrane translocation and mechanism for polarized signaling. Proc Natl Acad Sci U S A 2015;112:E267-276.
9 van Hennik PB, ten Klooster JP, Halstead JR, Voermans C, Anthony EC, Divecha N, Hordijk PL: The C-terminal domain of Rac1 contains two motifs that control targeting and signaling specificity. J Biol Chem 2003;278:39166-39175.
10 Finkielstein CV, Overduin M, Capelluto DG: Cell migration and signaling specificity is determined by the phosphatidylserine recognition motif of Rac1. J Biol Chem 2006;281:27317-27326.
11 Heo WD, Inoue T, Park WS, Kim ML, Park BO, Wandless TJ, Meyer T: PI(3,4,5)P3 and PI(4,5)P2 lipids target proteins with polybasic clusters to the plasma membrane. Science 2006;314:1458-1461.
12 Remorino A, De Beco S, Cayrac F, Di Federico F, Cornilleau G, Gautreau A, Parrini MC, Masson JB, Dahan M, Coppey M: Gradients of Rac1 Nanoclusters Support Spatial Patterns of Rac1 Signaling. Cell Rep 2017;21:1922-1935.
13 Fairn GD, Schieber NL, Ariotti N, Murphy S, Kuerschner L, Webb RI, Grinstein S, Parton RG: High-resolution mapping reveals topologically distinct cellular pools of phosphatidylserine. J Cell Biol 2011;194:257-275.
14 Kay JG, Koivusalo M, Ma X, Wohland T, Grinstein S: Phosphatidylserine dynamics in cellular membranes. Mol Biol Cell 2012;23:2198-2212.
15 Ehrlich JS, Hansen MD, Nelson WJ: Spatio-Temporal Regulation of Rac1 Localization and Lamellipodia Dynamics during Epithelial Cell-Cell Adhesion. Dev Cell 2002;3:259-270.
16 Machacek M, Hodgson L, Welch C, Elliott H, Pertz O, Nalbant P, Abell A, Johnson GL, Hahn KM, Danuser G: Coordination of Rho GTPase activities during cell protrusion. Nature 2009;461:99-103.
17 Ridley AJ: Life at the leading edge. Cell 2011;145:1012-1022.
18 Schwab A, Fabian A, Hanley PJ, Stock C: Role of ion channels and transporters in cell migration. Physiol Rev 2012;92:1865-1913.
19 Brackenbury WJ: Ion Channels in Cancer; in Pitt GS (ed) Ion Channels in Health and Disease, Elsevier Inc., 2016, pp 131-163.
20 Prevarskaya N, Skryma R, Shuba Y: Ion Channels in Cancer: Are Cancer Hallmarks Oncochannelopathies? Physiol Rev 2018;98:559-621.
21 Yang M, Brackenbury WJ: Membrane potential and cancer progression. Front Physiol 2013;4:185.

22 Sundelacruz S, Levin M, Kaplan DL: Role of membrane potential in the regulation of cell proliferation and differentiation. Stem Cell Rev 2009;5:231-246.
23 Blackiston DJ, McLaughlin KA, Levin M: Bioelectric controls of cell proliferation: ion channels, membrane voltage and the cell cycle. Cell Cycle 2009;8:3519-3528.
24 Zhou Y, Wong CO, Cho KJ, van der Hoeven D, Liang H, Thakur DP, Luo J, Babic M, Zinsmaier KE, Zhu MX, Hu H, Venkatachalam K, Hancock JF: Membrane potential modulates plasma membrane phospholipid dynamics and K-Ras signaling. Science 2015;349:873-876.
25 Sundelacruz S, Levin M, Kaplan DL: Membrane potential controls adipogenic and osteogenic differentiation of mesenchymal stem cells. PLoS One 2008;3:e3737.
26 Chifflet S, Hernandez JA, Grasso S: A possible role for membrane depolarization in epithelial wound healing. Am J Physiol Cell Physiol 2005;288:C1420-1430.
27 Chifflet S, Correa V, Nin V, Justet C, Hernandez JA: Effect of membrane potential depolarization on the organization of the actin cytoskeleton of eye epithelia. The role of adherens junctions. Exp Eye Res 2004;79:769-777.
28 Chifflet S, Hernandez JA, Grasso S, Cirillo A: Nonspecific depolarization of the plasma membrane potential induces cytoskeletal modifications of bovine corneal endothelial cells in culture. Exp Cell Res 2003;282:1-13.
29 Nin V, Hernandez JA, Chifflet S: Hyperpolarization of the plasma membrane potential provokes reorganization of the actin cytoskeleton and increases the stability of adherens junctions in bovine corneal endothelial cells in culture. Cell Motil Cytoskeleton 2009;66:1087-1099.
30 Szaszi K, Sirokmany G, Di Ciano-Oliveira C, Rotstein OD, Kapus A: Depolarization induces Rho-Rho kinase-mediated myosin light chain phosphorylation in kidney tubular cells. Am J Physiol Cell Physiol 2005;289:C673-685.
31 Beane WS, Morokuma J, Adams DS, Levin M: A chemical genetics approach reveals H,K-ATPase-mediated membrane voltage is required for planarian head regeneration. Chem Biol 2011;18:77-89.
32 Beane WS, Morokuma J, Lemire JM, Levin M: Bioelectric signaling regulates head and organ size during planarian regeneration. Development 2013;140:313-322.
33 Lobikin M, Chernet B, Lobo D, Levin M: Resting potential, oncogene-induced tumorigenesis, and metastasis: the bioelectric basis of cancer in vivo. Phys Biol 2012;9:065002.
34 Chernet BT, Levin M: Transmembrane voltage potential of somatic cells controls oncogene-mediated tumorigenesis at long-range. Oncotarget 2014;5:3287-3306.
35 Lobikin M, Lobo D, Blackiston DJ, Martyniuk CJ, Tkachenko E, Levin M: Serotonergic regulation of melanocyte conversion: A bioelectrically regulated network for stochastic all-or-none hyperpigmentation. Sci Signal 2015;8:ra99.
36 Cervera J, Alcaraz A, Mafe S: Bioelectrical Signals and Ion Channels in the Modeling of Multicellular Patterns and Cancer Biophysics. Sci Rep 2016;6:20403.
37 Chernet BT, Adams DS, Lobikin M, Levin M: Use of genetically encoded, light-gated ion translocators to control tumorigenesis. Oncotarget 2016
38 Catterall WA, Goldin AL, Waxman SG: International Union of Pharmacology. XXXIX. Compendium of voltage-gated ion channels: sodium channels. Pharmacol Rev 2003;55:575-578.
39 Brackenbury WJ, Isom LL: Na Channel beta Subunits: Overachievers of the Ion Channel Family. Front Pharmacol 2011;2:53.
40 Hille B: Ionic channels of excitable membranes, ed 2nd. Sunderland (Massachusetts), Sinauer Associates Inc., 1992.
41 Patel F, Brackenbury WJ: Dual roles of voltage-gated sodium channels in development and cancer. Int J Dev Biol 2015;59:357-366.
42 Brackenbury WJ, Calhoun JD, Chen C, Miyazaki H, Nukina N, Oyama F, Ranscht B, Isom LL: Functional reciprocity between Na+ channel Nav1.6 and β1 subunits in the coordinated regulation of excitability and neurite outgrowth. Proc Natl Acad Sci U S A 2010;107:2283-2288.

43 Brackenbury WJ, Yuan Y, O'Malley HA, Parent JM, Isom LL: Abnormal neuronal patterning occurs during early postnatal brain development of Scn1b-null mice and precedes hyperexcitability. Proc Natl Acad Sci U S A 2013;110:1089-1094.
44 Black JA, Waxman SG: Noncanonical roles of voltage-gated sodium channels. Neuron 2013;80:280-291.
45 Nelson M, Yang M, Dowle AA, Thomas JR, Brackenbury WJ: The sodium channel-blocking antiepileptic drug phenytoin inhibits breast tumour growth and metastasis. Mol Cancer 2015;14:13.
46 Nelson M, Yang M, Millican-Slater R, Brackenbury WJ: Nav1.5 regulates breast tumor growth and metastatic dissemination in vivo. Oncotarget 2015;6:32914-32929.
47 Martin F, Ufodiama C, Watt I, Bland M, Brackenbury WJ: Therapeutic value of voltage-gated sodium channel inhibitors in breast, colorectal and prostate cancer: a systematic review. Front Pharmacol 2015;6:273.
48 Brackenbury WJ, Chioni AM, Diss JK, Djamgoz MB: The neonatal splice variant of Nav1.5 potentiates in vitro metastatic behaviour of MDA-MB-231 human breast cancer cells. Breast Cancer Res Treat 2007;101:149-160.
49 Fraser SP, Diss JK, Chioni AM, Mycielska ME, Pan H, Yamaci RF, Pani F, Siwy Z, Krasowska M, Grzywna Z, Brackenbury WJ, Theodorou D, Koyuturk M, Kaya H, Battaloglu E, De Bella MT, Slade MJ, Tolhurst R, Palmieri C, Jiang J, Latchman DS, Coombes RC, Djamgoz MB: Voltage-gated sodium channel expression and potentiation of human breast cancer metastasis. Clin Cancer Res 2005;11:5381-5389.
50 Roger S, Besson P, Le Guennec JY: Involvement of a novel fast inward sodium current in the invasion capacity of a breast cancer cell line. Biochim Biophys Acta 2003;1616:107-111.
51 Brackenbury WJ: Voltage-gated sodium channels and metastatic disease. Channels (Austin) 2012;6:352-361.
52 Besson P, Driffort V, Bon E, Gradek F, Chevalier S, Roger S: How do voltage-gated sodium channels enhance migration and invasiveness in cancer cells? Biochim Biophys Acta 2015;1848:2493-2501.
53 Yang M, Kozminski DJ, Wold LA, Modak R, Calhoun JD, Isom LL, Brackenbury WJ: Therapeutic potential for phenytoin: targeting Na(v)1.5 sodium channels to reduce migration and invasion in metastatic breast cancer. Breast Cancer Res Treat 2012;134:603-615.
54 House CD, Vaske CJ, Schwartz A, Obias V, Frank B, Luu T, Sarvazyan N, Irby RB, Strausberg RL, Hales T, Stuart J, Lee NH: Voltage-gated Na+ channel SCN5A is a key regulator of a gene transcriptional network that controls colon cancer invasion. Cancer Res 2010;70:6957-6967.
55 House CD, Wang BD, Ceniccola K, Williams R, Simaan M, Olender J, Patel V, Baptista-Hon DT, Annunziata CM, Gutkind JS, Hales TG, Lee NH: Voltage-gated Na+ Channel Activity Increases Colon Cancer Transcriptional Activity and Invasion Via Persistent MAPK Signaling. Sci Rep 2015;5:11541.
56 Gillet L, Roger S, Besson P, Lecaille F, Gore J, Bougnoux P, Lalmanach G, Le Guennec JY: Voltage-gated Sodium Channel Activity Promotes Cysteine Cathepsin-dependent Invasiveness and Colony Growth of Human Cancer Cells. J Biol Chem 2009;284:8680-8691.
57 Brisson L, Driffort V, Benoist L, Poet M, Counillon L, Antelmi E, Rubino R, Besson P, Labbal F, Chevalier S, Reshkin SJ, Gore J, Roger S: NaV1.5 Na(+) channels allosterically regulate the NHE-1 exchanger and promote the activity of breast cancer cell invadopodia. J Cell Sci 2013;126:4835-4842.
58 Brisson L, Gillet L, Calaghan S, Besson P, Le Guennec JY, Roger S, Gore J: Na(V)1.5 enhances breast cancer cell invasiveness by increasing NHE1-dependent H(+) efflux in caveolae. Oncogene 2011;30:2070-2076.
59 Nelson M, Millican-Slater R, Forrest LC, Brackenbury WJ: The sodium channel beta1 subunit mediates outgrowth of neurite-like processes on breast cancer cells and promotes tumour growth and metastasis. Int J Cancer 2014;135:2338-2351.

60 Uphoff CC, Gignac SM, Drexler HG: Mycoplasma contamination in human leukemia cell lines. I. Comparison of various detection methods. J Immunol Methods 1992;149:43-53.
61 Masters JR, Thomson JA, Daly-Burns B, Reid YA, Dirks WG, Packer P, Toji LH, Ohno T, Tanabe H, Arlett CF, Kelland LR, Harrison M, Virmani A, Ward TH, Ayres KL, Debenham PG: Short tandem repeat profiling provides an international reference standard for human cell lines. Proc Natl Acad Sci U S A 2001;98:8012-8017.
62 Armstrong CM, Bezanilla F: Inactivation of the sodium channel. II. Gating current experiments. J Gen Physiol 1977;70:567-590.
63 Sanguinetti MC, Jurkiewicz NK: Two components of cardiac delayed rectifier K+ current. Differential sensitivity to block by class III antiarrhythmic agents. J Gen Physiol 1990;96:195-215.
64 Roger S, Rollin J, Barascu A, Besson P, Raynal PI, Iochmann S, Lei M, Bougnoux P, Gruel Y, Le Guennec JY: Voltage-gated sodium channels potentiate the invasive capacities of human non-small-cell lung cancer cell lines. Int J Biochem Cell Biol 2007;39:774-786.
65 Marrison J, Raty L, Marriott P, O'Toole P: Ptychography--a label free, high-contrast imaging technique for live cells using quantitative phase information. Sci Rep 2013;3:2369.
66 Suman R, Smith G, Hazel KE, Kasprowicz R, Coles M, O'Toole P, Chawla S: Label-free imaging to study phenotypic behavioural traits of cells in complex co-cultures. Sci Rep 2016;6:22032.
67 Schneider CA, Rasband WS, Eliceiri KW: NIH Image to ImageJ: 25 years of image analysis. Nat Methods 2012;9:671-675.
68 Dang I, Gorelik R, Sousa-Blin C, Derivery E, Guerin C, Linkner J, Nemethova M, Dumortier JG, Giger FA, Chipysheva TA, Ermilova VD, Vacher S, Campanacci V, Herrada I, Planson AG, Fetics S, Henriot V, David V, Oguievetskaia K, Lakisic G, Pierre F, Steffen A, Boyreau A, Peyrieras N, Rottner K, Zinn-Justin S, Cherfils J, Bieche I, Alexandrova AY, David NB, Small JV, Faix J, Blanchoin L, Gautreau A: Inhibitory signalling to the Arp2/3 complex steers cell migration. Nature 2013;503:281-284.
69 Manders EMM, Verbeek FJ, Aten JA: Measurement of co-localization of objects in dual-colour confocal images. J Microsc 1993;169:375-382.
70 Li Q, Lau A, Morris TJ, Guo L, Fordyce CB, Stanley EF: A syntaxin 1, Galpha(o), and N-type calcium channel complex at a presynaptic nerve terminal: analysis by quantitative immunocolocalization. J Neurosci 2004;24:4070-4081.
71 Antonov AS, Antonova GN, Fujii M, ten Dijke P, Handa V, Catravas JD, Verin AD: Regulation of endothelial barrier function by TGF-beta type I receptor ALK5: potential role of contractile mechanisms and heat shock protein 90. J Cell Physiol 2012;227:759-771.
72 Fritz RD, Menshykau D, Martin K, Reimann A, Pontelli V, Pertz O: SrGAP2-Dependent Integration of Membrane Geometry and Slit-Robo-Repulsive Cues Regulates Fibroblast Contact Inhibition of Locomotion. Dev Cell 2015;35:78-92.
73 George AL, Jr.: Inherited disorders of voltage-gated sodium channels. J Clin Invest 2005;115:1990-1999.
74 Ulbricht W: Effects of veratridine on sodium currents and fluxes. Rev Physiol Biochem Pharmacol 1998;133:1-54.
75 Campbell TM, Main MJ, Fitzgerald EM: Functional expression of the voltage-gated Na(+)-channel Nav1.7 is necessary for EGF-mediated invasion in human non-small cell lung cancer cells. J Cell Sci 2013;126:4939-4949.
76 Contreras GF, Castillo K, Enrique N, Carrasquel-Ursulaez W, Castillo JP, Milesi V, Neely A, Alvarez O, Ferreira G, Gonzalez C, Latorre R: A BK (Slo1) channel journey from molecule to physiology. Channels (Austin) 2013;7:442-458.
77 Khaitan D, Sankpal UT, Weksler B, Meister EA, Romero IA, Couraud PO, Ningaraj NS: Role of KCNMA1 gene in breast cancer invasion and metastasis to brain. BMC Cancer 2009;9:258.
78 Ma YG, Liu WC, Dong S, Du C, Wang XJ, Li JS, Xie XP, Wu L, Ma DC, Yu ZB, Xie MJ: Activation of BK(Ca) channels in zoledronic acid-induced apoptosis of MDA-MB-231 breast cancer cells. PLoS One 2012;7:e37451.

79 Roger S, Potier M, Vandier C, Le Guennec JY, Besson P: Description and role in proliferation of iberiotoxin-sensitive currents in different human mammary epithelial normal and cancerous cells. Biochim Biophys Acta 2004;1667:190-199.
80 Macmillan S, Sheridan RD, Chilvers ER, Patmore L: A comparison of the effects of SCA40, NS 004 and NS 1619 on large conductance Ca(2+)-activated K+ channels in bovine tracheal smooth muscle cells in culture. Br J Pharmacol 1995;116:1656-1660.
81 Winnicka K, Bielawski K, Bielawska A, Surazynski A: Antiproliferative activity of derivatives of ouabain, digoxin and proscillaridin A in human MCF-7 and MDA-MB-231 breast cancer cells. Biol Pharm Bull 2008;31:1131-1140.
82 Sareen D, Darjatmoko SR, Albert DM, Polans AS: Mitochondria, calcium, and calpain are key mediators of resveratrol-induced apoptosis in breast cancer. Mol Pharmacol 2007;72:1466-1475.
83 Driffort V, Gillet L, Bon E, Marionneau-Lambot S, Oullier T, Joulin V, Collin C, Pages JC, Jourdan ML, Chevalier S, Bougnoux P, Le Guennec JY, Besson P, Roger S: Ranolazine inhibits NaV1.5-mediated breast cancer cell invasiveness and lung colonization. Mol Cancer 2014;13:264.
84 Burridge K, Wennerberg K: Rho and Rac take center stage. Cell 2004;116:167-179.
85 Moissoglu K, Slepchenko BM, Meller N, Horwitz AF, Schwartz MA: In Vivo Dynamics of Rac-Membrane Interactions. Mol Biol Cell 2006;17:2770-2779.
86 Magalhaes MAO, Glogauer M: Pivotal Advance: Phospholipids determine net membrane surface charge resulting in differential localization of active Rac1 and Rac2. J Leukoc Biol 2010;87:545-555.
87 Djamgoz MB, Onkal R: Persistent current blockers of voltage-gated sodium channels: a clinical opportunity for controlling metastatic disease. Recent Pat Anticancer Drug Discov 2013;8:66-84.
88 Stys PK, Sontheimer H, Ransom BR, Waxman SG: Noninactivating, tetrodotoxin-sensitive Na+ conductance in rat optic nerve axons. Proc Natl Acad Sci U S A 1993;90:6976-6980.
89 Sontheimer H, Fernandez-Marques E, Ullrich N, Pappas CA, Waxman SG: Astrocyte Na+ channels are required for maintenance of Na+/K(+)-ATPase activity. J Neurosci 1994;14:2464-2475.
90 Amara S, Ivy MT, Myles EL, Tiriveedhi V: Sodium channel gammaENaC mediates IL-17 synergized high salt induced inflammatory stress in breast cancer cells. Cell Immunol 2015
91 Baylor DA, Fettiplace R: Transmission from photoreceptors to ganglion cells in turtle retina. J Physiol 1977;271:391-424.
92 Cone CD, Jr., Cone CM: Induction of mitosis in mature neurons in central nervous system by sustained depolarization. Science 1976;192:155-158.
93 Cone CD, Jr.: Maintenance of mitotic homeostasis in somatic cell populations. J Theor Biol 1971;30:183-194.
94 Kraft R, Krause P, Jung S, Basrai D, Liebmann L, Bolz J, Patt S: BK channel openers inhibit migration of human glioma cells. Pflugers Arch 2003;446:248-255.
95 Waheed F, Speight P, Kawai G, Dan Q, Kapus A, Szaszi K: Extracellular signal-regulated kinase and GEF-H1 mediate depolarization-induced Rho activation and paracellular permeability increase. Am J Physiol Cell Physiol 2010;298:C1376-1387.
96 Persson AK, Estacion M, Ahn H, Liu S, Stamboulian-Platel S, Waxman SG, Black JA: Contribution of sodium channels to lamellipodial protrusion and Rac1 and ERK1/2 activation in ATP-stimulated microglia. Glia 2014;62:2080-2095.
97 Baldassa S, Zippel R, Sturani E: Depolarization-induced signaling to Ras, Rap1 and MAPKs in cortical neurons. Brain Res Mol Brain Res 2003;119:111-122.
98 Servitja JM, Marinissen MJ, Sodhi A, Bustelo XR, Gutkind JS: Rac1 function is required for Src-induced transformation. Evidence of a role for Tiam1 and Vav2 in Rac activation by Src. J Biol Chem 2003;278:34339-34346.
99 Lee JL, Wang MJ, Sudhir PR, Chen JY: CD44 engagement promotes matrix-derived survival through the CD44-SRC-integrin axis in lipid rafts. Mol Cell Biol 2008;28:5710-5723.

100 Bourguignon LY, Zhu H, Shao L, Chen YW: CD44 interaction with c-Src kinase promotes cortactin-mediated cytoskeleton function and hyaluronic acid-dependent ovarian tumor cell migration. J Biol Chem 2001;276:7327-7336.
101 Pappalardo LW, Samad OA, Black JA, Waxman SG: Voltage-gated sodium channel Nav 1.5 contributes to astrogliosis in an in vitro model of glial injury via reverse Na+ /Ca2+ exchange. Glia 2014;62:1162-1175.
102 Black JA, Dib-Hajj S, Cohen S, Hinson AW, Waxman SG: Glial cells have heart: rH1 Na+ channel mRNA and protein in spinal cord astrocytes. Glia 1998;23:200-208.
103 Carrithers MD, Dib-Hajj S, Carrithers LM, Tokmoulina G, Pypaert M, Jonas EA, Waxman SG: Expression of the voltage-gated sodium channel NaV1.5 in the macrophage late endosome regulates endosomal acidification. J Immunol 2007;178:7822-7832.
104 Carrithers MD, Chatterjee G, Carrithers LM, Offoha R, Iheagwara U, Rahner C, Graham M, Waxman SG: Regulation of podosome formation in macrophages by a novel splice variant of the sodium channel SCN8A. J Biol Chem 2009;284:8114-8126.
105 Black JA, Liu S, Waxman SG: Sodium channel activity modulates multiple functions in microglia. Glia 2009;57:1072-1081.
106 Fraser SP, Ding Y, Liu A, Foster CS, Djamgoz MB: Tetrodotoxin suppresses morphological enhancement of the metastatic MAT-LyLu rat prostate cancer cell line. Cell Tissue Res 1999;295:505-512.
107 Brackenbury WJ, Djamgoz MB: Activity-dependent regulation of voltage-gated Na^+ channel expression in Mat-LyLu rat prostate cancer cell line. J Physiol 2006;573:343-356.
108 Yildirim S, Altun S, Gumushan H, Patel A, Djamgoz MB: Voltage-gated sodium channel activity promotes prostate cancer metastasis in vivo. Cancer Lett 2012;323:58-61.
109 Pollard TD: Regulation of actin filament assembly by Arp2/3 complex and formins. Annu Rev Biophys Biomol Struct 2007;36:451-477.
110 Stock C, Schwab A: Ion channels and transporters in metastasis. Biochim Biophys Acta 2015;1848:2638-2646.

Figure legends

Figure 1. $Na_v1.5$ is endogenously expressed in breast carcinoma cells and regulates the membrane potential. (A) MDA-MB-231 cells labeled with $Na_v1.5$ antibody (green), phalloidin to label the actin cytoskeleton (red), and DAPI to label the nucleus (blue). Insets show cell peripheries at higher magnification. (B) Typical whole-cell recording showing large transient and small persistent Na^+ current. The cell was depolarized to -10 mV for 50 ms following a 250 ms pre-pulse at -120 mV. (C) Expanded view of persistent Na^+ current 40-45 ms following onset of depolarization. (D) Activation and steady-state inactivation of Na^+ current. Normalized conductance (G/G_{Max}) was calculated from the current data and plotted as a function of voltage (n = 14). Normalized current (I/I_{Max}) was plotted as a function of the pre-pulse voltage (n = 9). Data are fitted with Boltzmann functions. (E) Expanded view of shaded area under activation and inactivation traces highlighting the window current. (F) Effect of $Na_v1.5$ shRNA knock-down on the V_m compared to non-targeting shRNA control (n = 16). Data are mean and SEM. *P < 0.05; **P < 0.01; Student's t-test.

Figure 2. Tetrodotoxin hyperpolarizes, and veratridine depolarizes, the membrane potential. (A) Representative trace showing the inhibitory effect of tetrodotoxin (TTX; 30 μM) on Na^+ current, and recovery after washout. The cell was held at -120 mV for 250 ms before depolarizing to -10 mV for 50 ms. (B) Expanded view of persistent Na^+ current 40-45 ms following onset of depolarization. (C) Quantification of the normalized transient Na^+ current after TTX (30 μM) treatment and following washout (n = 7). (D) Quantification of the normalized persistent Na^+ current after TTX (30 μM) treatment and following washout (n = 4). (E) V_m in control physiological saline solution, after TTX (30 μM) treatment and following washout. Solid line, mean; gray shading, SEM (n = 17). (F) Quantification of V_m over the last 5 s in control, TTX, and washout (n = 17). (G) Representative trace showing effect of veratridine (100 μM) on Na^+ current. The cell was held at -120 mV for 250 ms before depolarizing to 0 mV for 50 ms. (H) Expanded view of persistent Na^+ current 40-45 ms

following onset of depolarization. (I) V_m in control PSS and 120 s after perfusion with veratridine (n = 13). Data are mean and SEM. **P < 0.01; ***P < 0.001; repeated measures ANOVA with Tukey test for (C), (D), (F); Student's t test for (I).

Figure 3. Extracellular Na^+ sets the membrane potential and intracellular Na^+ level. (A) V_m in control physiological saline solution, after extracellular Na^+ replacement with choline chloride and following washout. Solid line, mean; gray shading, SEM (n = 10). (B) Quantification of V_m over the last 5 s in control, choline chloride, and washout (n = 10). (C) Representative SBFI fluorescence intensity (ratio of emission at 340 nm/380 nm) when cells were perfused with standard physiological saline (center panel), solution containing 10 mM Na^+ and 20 μM gramicidin (left panel) and solution containing 20 mM Na^+ and 20 μM gramicidin (right panel). Ratio images are color-coded so that warm and cold colors represent high and low $[Na^+]$, respectively. Scale bar = 10 μm. (D) Calibration of relationship between SBFI fluorescence intensity (340/380 ratio) and $[Na^+]_i$. Dashed line, linear regression (r^2 = 0.99; n = 40). (E) Quantification steady-state $[Na^+]_i$ in control physiological saline solution (n = 6), when extracellular Na^+ was replaced with NMDG (n = 3), and in TTX (30 μM; n = 3). (F) Effect of $Na_v1.5$ shRNA knock-down on $[Na^+]_i$ compared to non-targeting shRNA control (n = 3). Data are mean and SEM. *P < 0.05; **P < 0.01; ***P < 0.001; ANOVA with Tukey post hoc test for (A) and (E); Student's t test for (F).

Figure 4. The large conductance Ca^{2+}-activated K^+ channel $K_{Ca}1.1$ regulates the membrane potential but not intracellular Na^+. (A) MDA-MB-231 cells labeled with $K_{Ca}1.1$ antibody (green), phalloidin to label the actin cytoskeleton (red), and DAPI to label the nucleus (blue). (B) Western blot of KCa1.1 in control MDA-MB-231 cells and cells in which Nav1.5 has been knocked down with shRNA. Positive control = rat brain lysate. Loading control = α-tubulin. (C) Representative perforated patch clamp recording showing activation of outward current using the KCa1.1 activator (NS-1619; 1 μM) and inhibition with iberiotoxin (100 nM). The cell

was held at -120 mV for 250 ms before depolarization to +60 mV for 300 ms. (D) Current-voltage relationship of the $K_{Ca}1.1$ current. Cells were held at -120 mV for 250 ms before depolarization to voltages ranging from -60 to +90 mV in 10 mV steps for 300 ms (n = 5). Data are fitted with single exponential functions. (E) Dose-dependent effect of NS-1619 on the steady-state V_m (n ≥ 6). Data are fitted to a sigmoidal logistic function. (F) Effect of NS-1619 (1 μM) on steady-state V_m (n = 12). (G) Effect of NS-1619 (1 μM, 5 min) on $[Na^+]_i$ (n = 22). (H) V_m recorded using intracellular solution with free $[Ca^{2+}]$ buffered to 5.7 nM *vs.* 100 nM (n ≥ 10). Data are mean and SEM. **P < 0.01; Student's paired t-test.

Figure 5. $Na_v1.5$-dependent membrane potential depolarization regulates cell migration. (A) Representative scratch wounds at 0 h and 6 h into a wound healing assay ± TTX (30 μM) or NS-1619 (1 μM). Red dotted lines highlight wound edges. (B) Wound area during the migration assay ("gap remaining"), normalized to starting value (n = 3). (C) $t_{1/2}$ of wound closure (n ≥ 5). (D) Collective migration (μm/h) of cells closing the wound (n ≥ 5). (E) Instantaneous velocity (μm/s) of segmented cells (n ≥ 2662). (F) Polar histograms showing directionality of migrating cells at the leading edge of wounds (P <0.001; Friedman with Dunn's test). 90˚ = axis perpendicular to wound. Data in (B – D) are mean and SEM. Box plot whiskers in (E) show maximum and minimum values and horizontal lines show 75th, 50th, and 25th percentile values. *P < 0.05; **P < 0.01; ***P <0.001; ANOVA with Tukey test (C, D); Kruskal-Wallis with Dunn's test (E).

Figure 6. $Na_v1.5$-dependent membrane potential depolarization regulates lamellipodia formation. (A) Images of representative cells after treatment with TTX (30 μM) or NS-1619 (1 μM) for 3 h. Cells were fixed and stained with phalloidin (red) and DAPI (blue). Lower row shows masks of cells in the upper row, from which the circularity was calculated. (B) Circularity (n ≥ 61). (C) Feret's diameter (μm; n ≥ 57). (D) Number of MDA-MB-231 cells with

a lamellipodium (P < 0.001; χ^2 test). Bars in (B) and (C) are mean and SEM. *P < 0.05; **P < 0.01; ***P < 0.001; ANOVA with Tukey test.

Figure 7. $Na_v1.5$ and V_m regulate Rac1 activation/distribution. (A) Images of representative cells after treatment with TTX (30 μM) and NS-1619 (1 μM) for 3 h. Cells were labeled with Rac1-GTP antibody (green), phalloidin (red) and DAPI (blue). Arrows in the Rac1-GTP panels highlight the distribution or lack of expression at the leading edge. (B) Rac1-GTP signal density, measured across 20 arcs, in 0.43 μm radius increments, within a quadrant mask region of interest at the leading edge, normalized to the first arc (n ≥ 66). (C) Peak Rac1-GTP signal density per cell from (B), normalized to the first arc (n ≥ 66). (D) Total Rac1-GTP quantified in whole cell lysates using colorimetric small GTPase activation assay (n = 6). (E) Images of representative cells after treatment with TTX (30 μM) and NS-1619 (1 μM) for 3 h. Cells were labeled with Rac1-GTP antibody (green), total Rac1 antibody (red), and DAPI (blue). Arrows in the Rac1-GTP panels highlight the distribution or lack of expression at the leading edge. (F) Total Rac1 signal density, measured across 20 arcs, in 0.43 μm radius increments, within a quadrant mask region of interest at the leading edge, normalized to the first arc (n ≥ 59). (G) Peak Rac1-GTP signal density per cell from (F), normalized to the first arc (n ≥ 59). (H) Ratio of Peak Rac1-GTP/Peak total Rac1 for each experimental repeat, normalized to control (n = 3). Data are mean and SEM. *P < 0.05; **P < 0.01; ***P < 0.001; ANOVA with Tukey test.

Figure 8. $Na_v1.5$ and V_m regulate Rac1-GTP colocalization with phosphatidylserine. (A) Images of representative cells after treatment with TTX (30 μM) and NS-1619 (1 μM) for 3 h. Cells were labeled with Rac1-GTP antibody (green), annexin V (red) and DAPI (blue). Dashed lines highlight regions of interest at the leading edge. (B) Cytofluorogram showing colocalization of annexin V and Rac1-GTP staining in region of interest in control cell from (A), normalized to maximum in each channel. (C) Cytofluorogram showing colocalization of

annexin V and Rac1-GTP staining in region of interest in TTX cell from (A), normalized to maximum in each channel. (D) Cytofluorogram showing colocalization of annexin V and Rac1-GTP staining in region of interest in NS-1619 cell from (A), normalized to maximum in each channel. (E) Manders' corrected colocalization coefficients for annexin V and Rac1-GTP staining in regions of interest of cells after treatment with TTX (30 μM) and NS-1619 (1 μM) for 3 h (n = 30). (F) Li's intensity correlation quotient for Rac1-GTP and annexin V colocalization (n = 30). Data are mean and SEM. **P < 0.01; ***P < 0.001; ANOVA with Tukey test.

Figure 9. $Na_v1.5$ regulates Rac1 activation in live cells detected using a genetically encoded Rac1 FRET biosensor. (A) Images of representative cells after treatment ± TTX (30 μM) for 3 h. Rac1 activation biosensor distribution is shown in the donor (mTFP) channel. Images are color-coded so that warm and cold colors represent high and low values, respectively, for sensor distribution and activation (FRET). (B) Fluorescence intensity profile along line drawn across control cell in (A). (C) Fluorescence intensity profile along line drawn across TTX-treated cell in (A). (D) Emission ratio (FRET), for cells measured after treatment ± TTX (30 μM) for 3 h, normalized to control (n ≥ 33). Data are mean and SEM. **P < 0.01; Student's t test.

Figure 10. $Na_v1.5$-mediated morphological changes and migration are dependent on Rac1 activation. (A) Images of representative cells after treatment with TTX (30 μM) ± Rac1 inhibitor (EHT1864; 0.5 μM) for 3 h. Cells are labeled with CD44 antibody (red). (B) Circularity of cells after treatment with TTX (30 μM) ± EHT1864 (0.5 μM) for 3 h (n ≥ 308). (C) Feret's diameter (μm) of cells after treatment with TTX (30 μM) ± EHT1864 (0.5 μM) for 3 h (n ≥ 308). Data are mean and SEM. ***P < 0.001; ANOVA with Tukey test. (D) Proposed mechanism underlying $Na_v1.5$-mediated V_m-dependent morphological changes and migration. $Na_v1.5$ channels carry Na^+ influx, which depolarizes the V_m, causing redistribution of charged phosphatidylserine in the inner leaflet of the phospholipid bilayer, promoting

Rac1 redistribution and activation. Rac1 regulates cytoskeletal modification *via* the Arp2/3 complex and increasing phosphorylation of cortactin and cofilin, promoting acquisition of a promigratory phenotype [109, 110]. Na^+ influx through $Na_v1.5$ channels may also impact on migration and invasion through other mechanism(s), including via β1 subunit-dependent adhesion [54, 55, 57, 59].

Figure 1

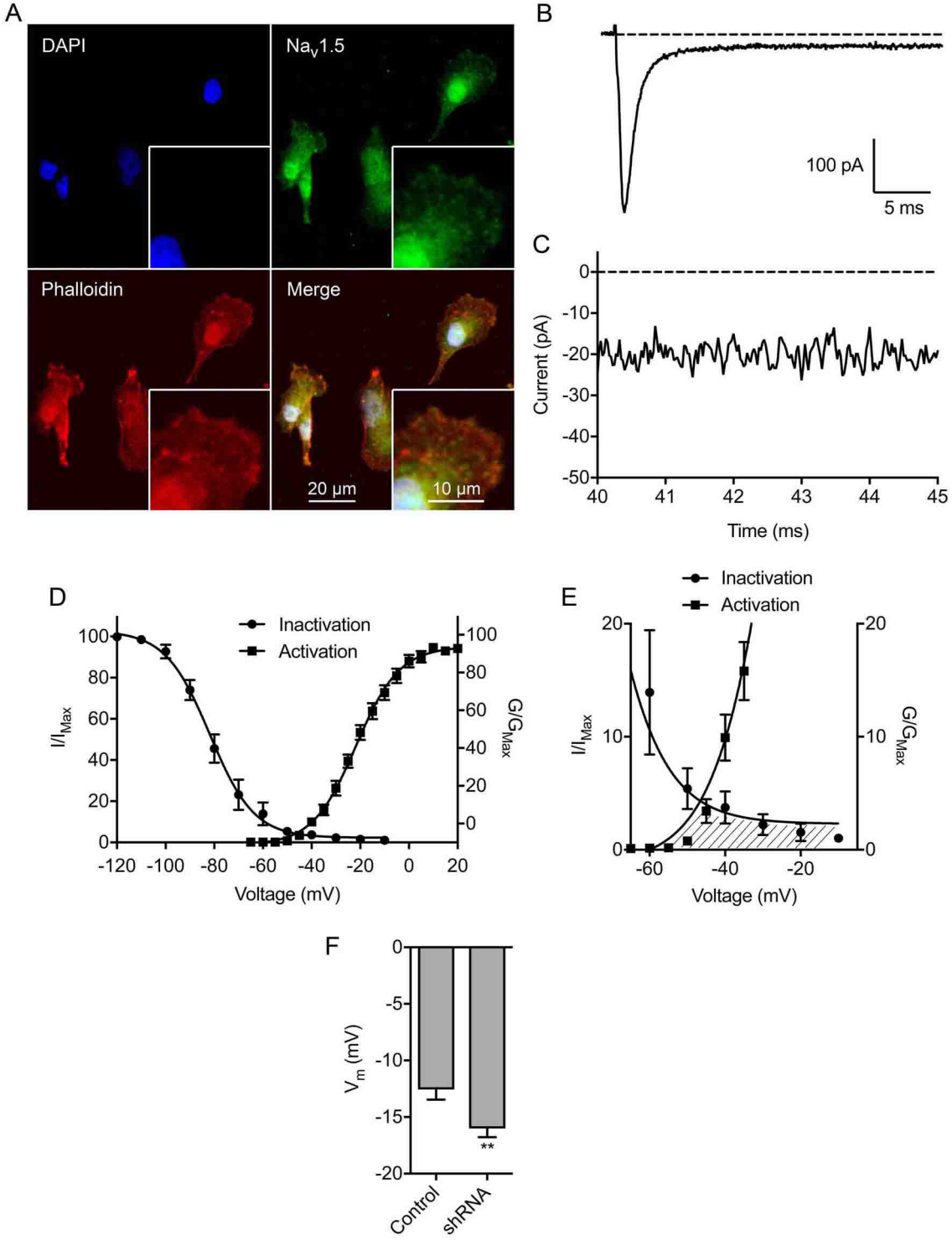
A
DAPI
Na$_V$1.5
Phalloidin
Merge
20 µm
10 µm
B
100 pA
5 ms
C
Current (pA)
0
-10
-20
-30
-40
-50
40
41
42
43
44
45
Time (ms)
D
Inactivation
Activation
I/I$_{Max}$
G/G$_{Max}$
100
80
60
40
20
0
-120
-100
-80
-60
-40
-20
0
20
Voltage (mV)
E
Inactivation
Activation
I/I$_{Max}$
G/G$_{Max}$
20
10
0
-60
-40
-20
Voltage (mV)
F
V$_m$ (mV)
0
-5
-10
-15
-20
**
Control
shRNA

Figure 2

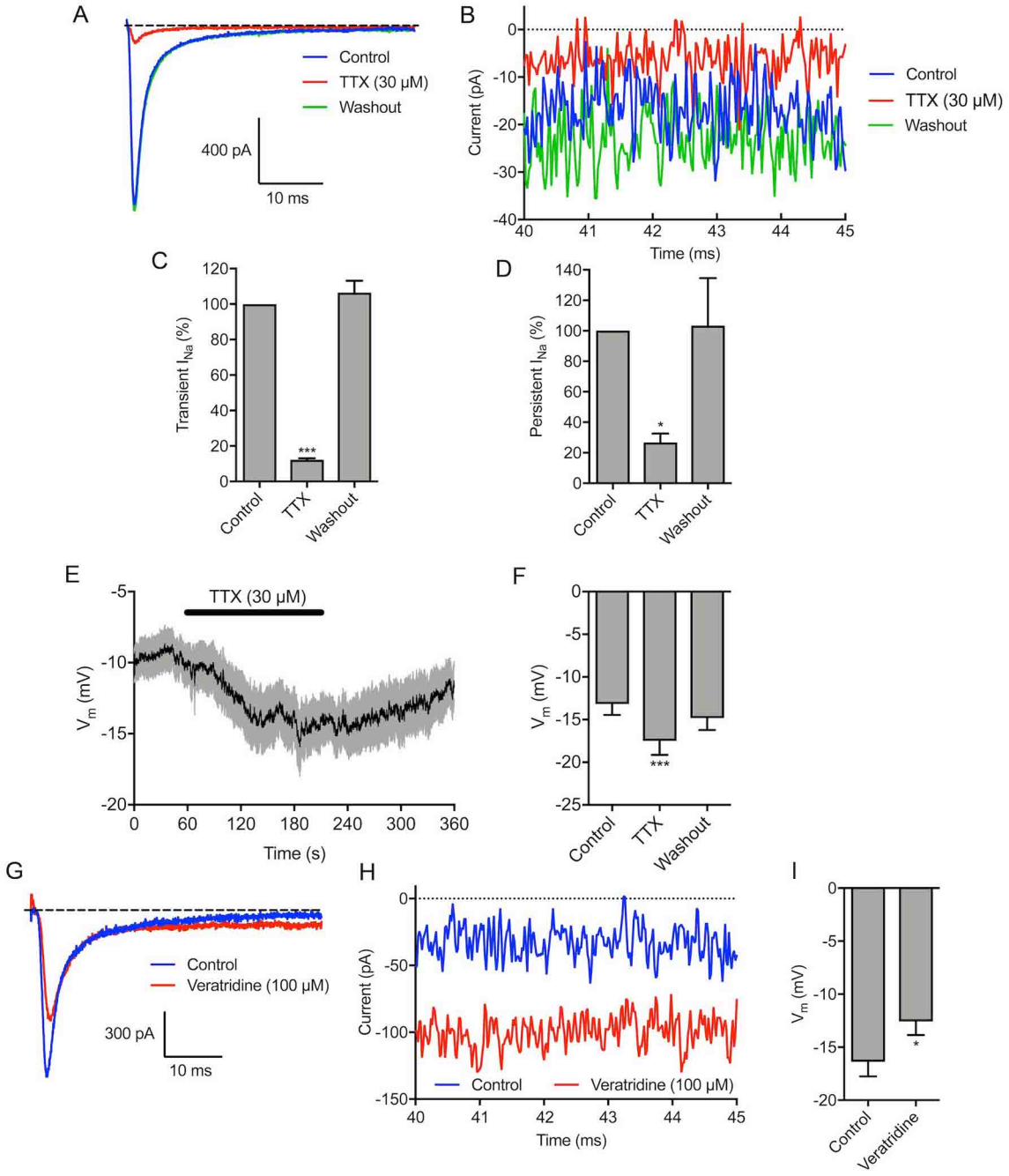
A
Control
TTX (30 μM)
Washout
400 pA
10 ms
B
Current (pA)
Time (ms)
Control
TTX (30 μM)
Washout
C
Transient I_{Na} (%)
***
Control
TTX
Washout
D
Persistent I_{Na} (%)
*
Control
TTX
Washout
E
TTX (30 μM)
V_m (mV)
Time (s)
F
V_m (mV)
***
Control
TTX
Washout
G
Control
Veratridine (100 μM)
300 pA
10 ms
H
Current (pA)
Control
Veratridine (100 μM)
Time (ms)
I
V_m (mV)
*
Control
Veratridine

Figure 3

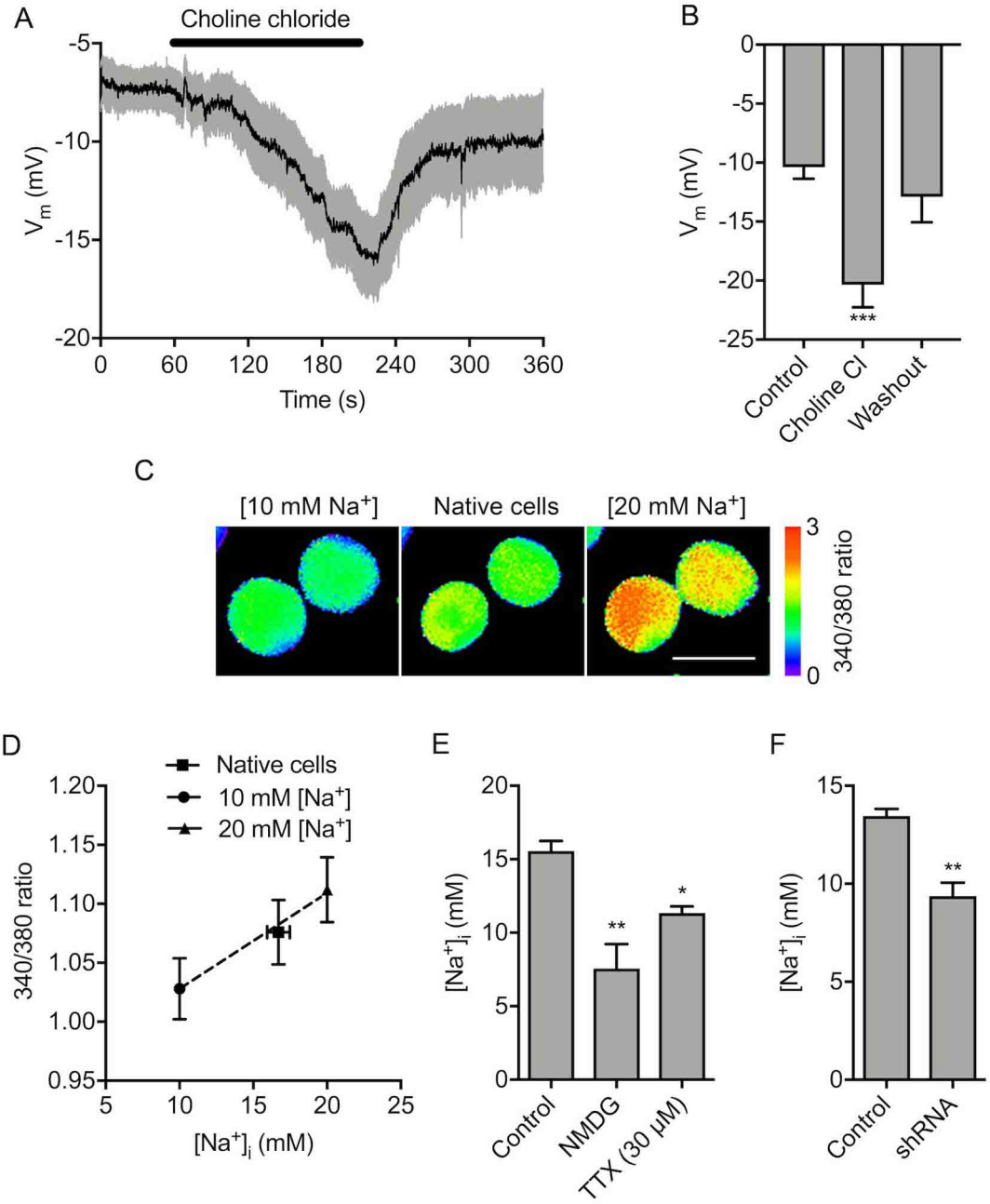
A
Choline chloride
-5
-10
-15
-20
V_m (mV)
0
60
120
180
240
300
360
Time (s)
B
0
-5
-10
-15
-20
-25
V_m (mV)
***
Control
Choline Cl
Washout
C
[10 mM Na+]
Native cells
[20 mM Na+]
3
0
340/380 ratio
D
Native cells
10 mM [Na+]
20 mM [Na+]
1.20
1.15
1.10
1.05
1.00
0.95
340/380 ratio
5
10
15
20
25
$[Na^+]_i$ (mM)
E
20
15
10
5
0
$[Na^+]_i$ (mM)
**
*
Control
NMDG
TTX (30 μM)
F
15
10
5
0
$[Na^+]_i$ (mM)
**
Control
shRNA

Figure 4

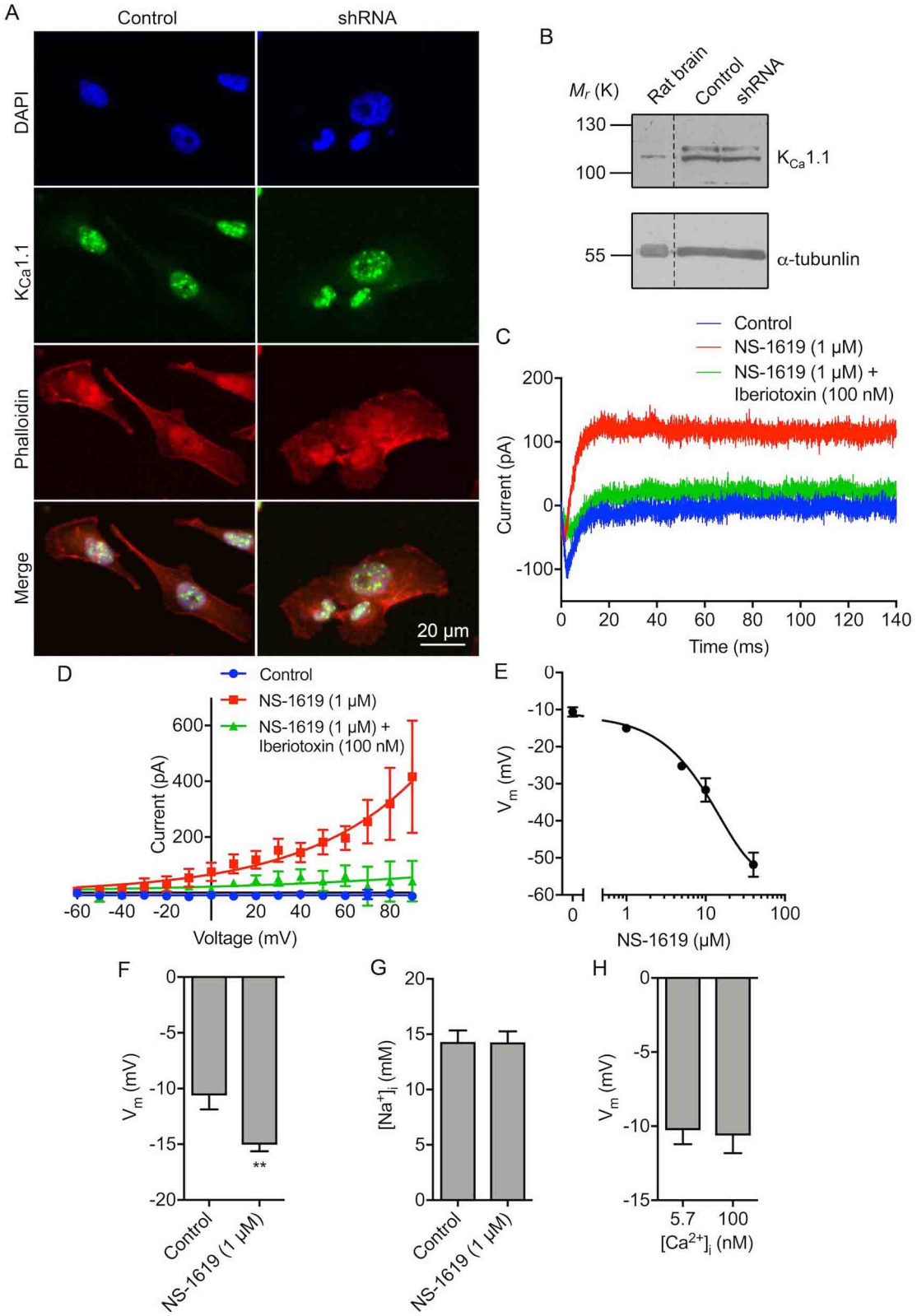
A
Control
shRNA
DAPI
KCa1.1
Phalloidin
Merge
20 μm
B
Mr (K)
Rat brain
Control
shRNA
130
100
KCa1.1
55
α-tubunlin
C
Control
NS-1619 (1 μM)
NS-1619 (1 μM) +
Iberiotoxin (100 nM)
Current (pA)
Time (ms)
D
Control
NS-1619 (1 μM)
NS-1619 (1 μM) +
Iberiotoxin (100 nM)
Current (pA)
Voltage (mV)
E
Vm (mV)
NS-1619 (μM)
F
Vm (mV)
**
Control
NS-1619 (1 μM)
G
[Na+]i (mM)
Control
NS-1619 (1 μM)
H
Vm (mV)
5.7
100
[Ca2+]i (nM)

Figure 5

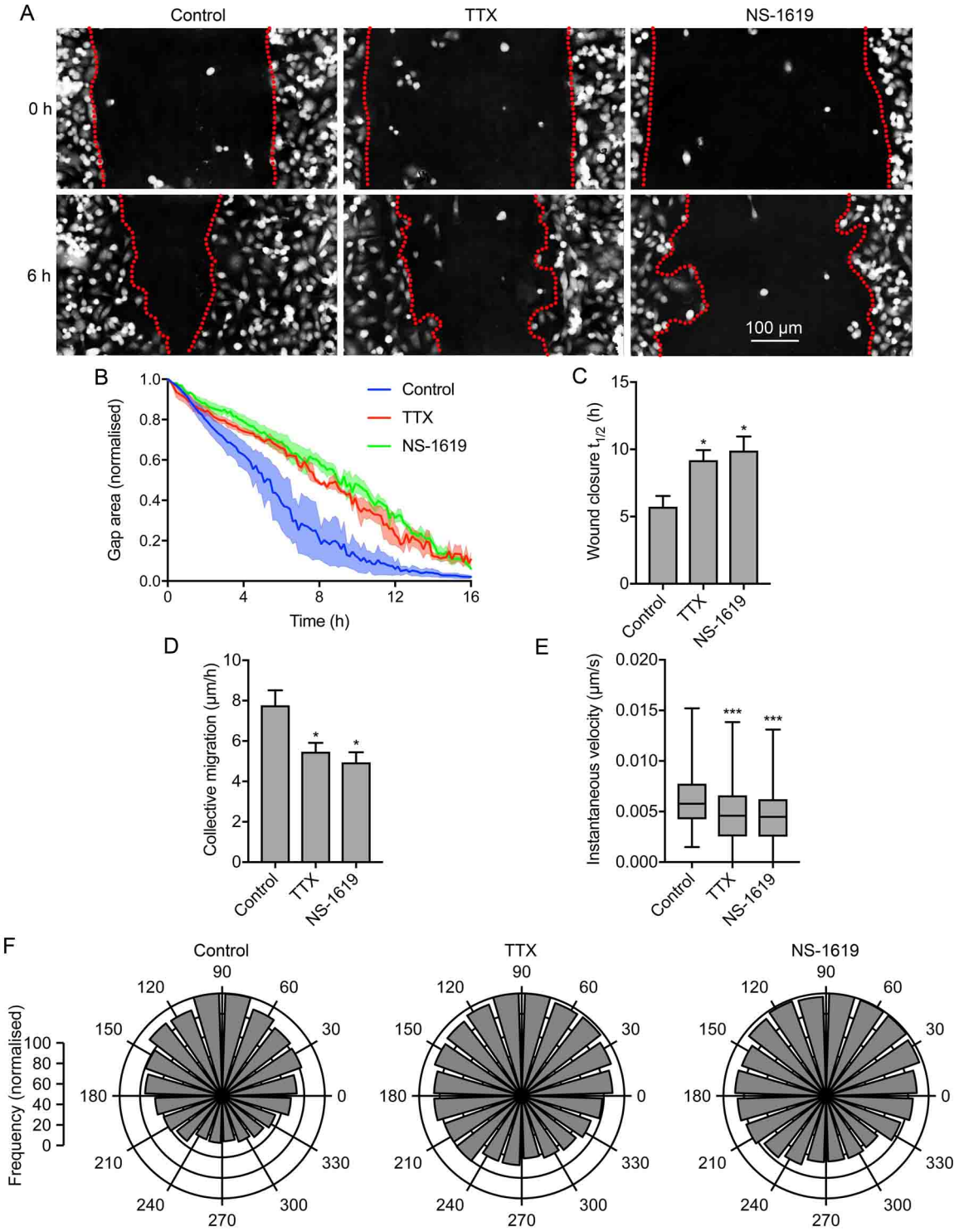
A
Control
TTX
NS-1619
0 h
6 h
100 µm
B
Gap area (normalised)
Time (h)
Control
TTX
NS-1619
C
Wound closure $t_{1/2}$ (h)
Control
TTX
NS-1619
D
Collective migration (µm/h)
Control
TTX
NS-1619
E
Instantaneous velocity (µm/s)
Control
TTX
NS-1619
F
Frequency (normalised)
Control
TTX
NS-1619

Figure 6

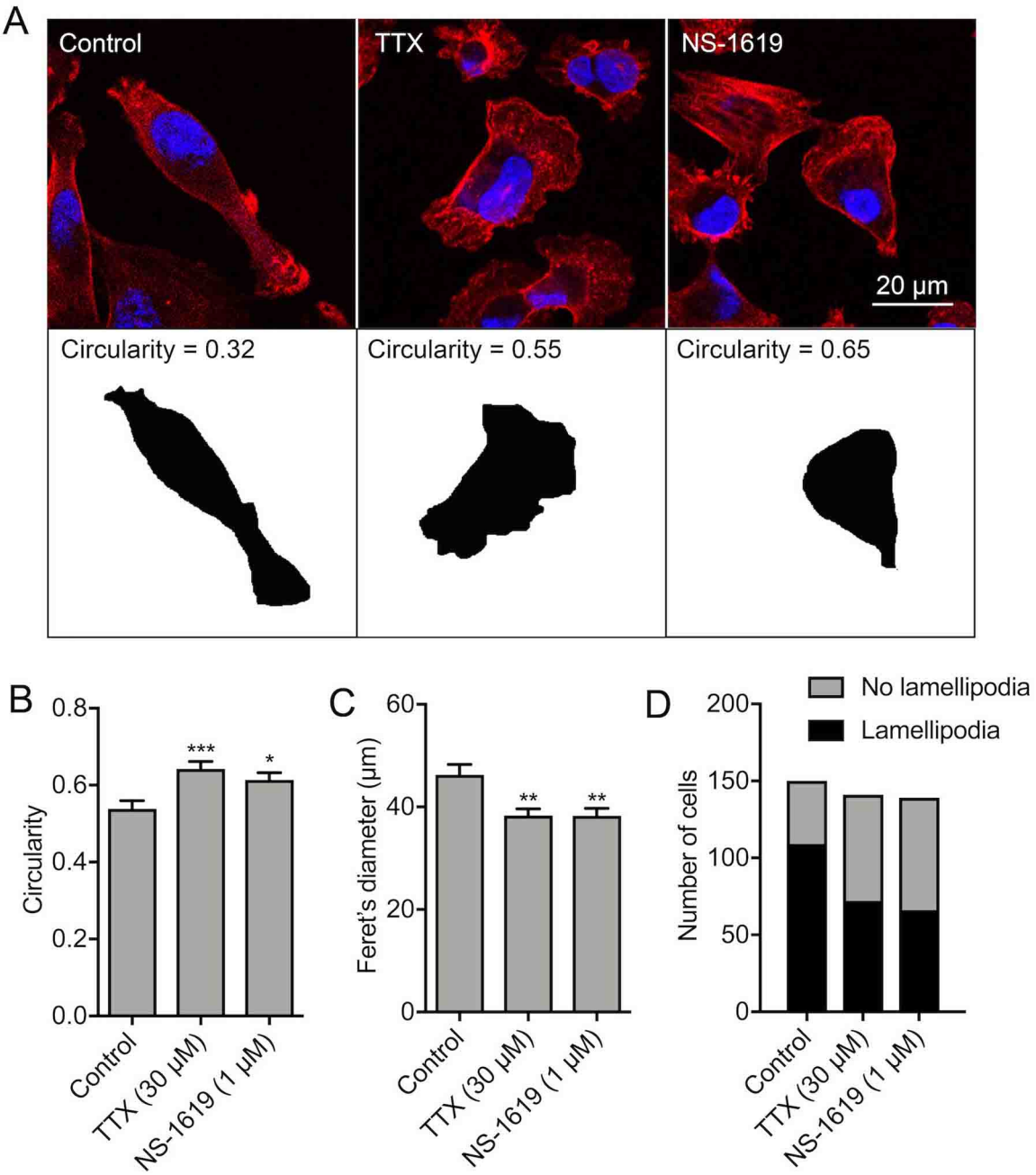
A
Control
TTX
NS-1619
20 µm
Circularity = 0.32
Circularity = 0.55
Circularity = 0.65
B
Circularity
0.0
0.2
0.4
0.6
0.8
***
*
Control
TTX (30 µM)
NS-1619 (1 µM)
C
Feret's diameter (µm)
0
20
40
60
**
**
Control
TTX (30 µM)
NS-1619 (1 µM)
D
No lamellipodia
Lamellipodia
Number of cells
0
50
100
150
200
Control
TTX (30 µM)
NS-1619 (1 µM)

Figure 7

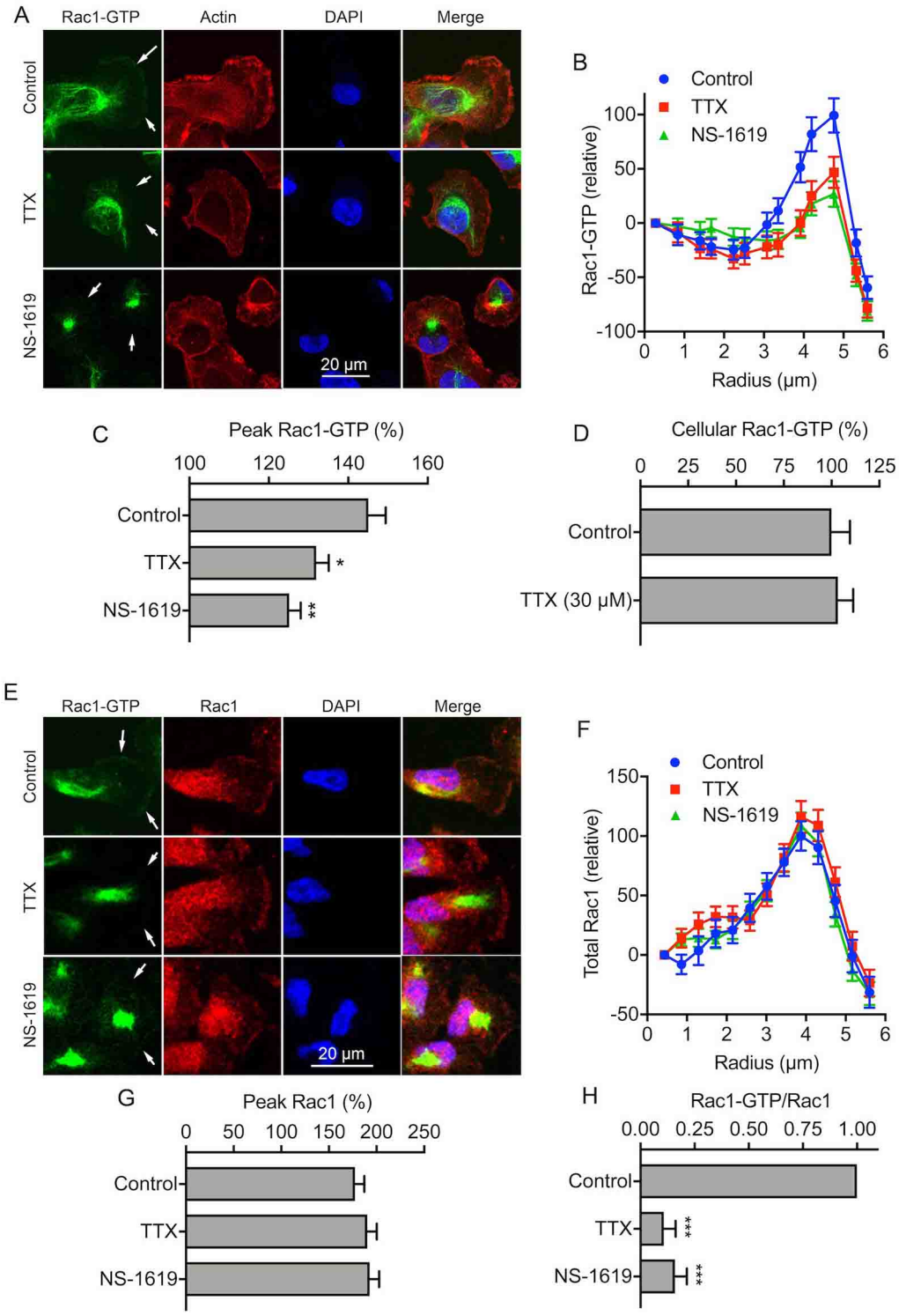
A
Rac1-GTP
Actin
DAPI
Merge
Control
TTX
NS-1619
20 µm
B
Control
TTX
NS-1619
Rac1-GTP (relative)
Radius (µm)
C
Peak Rac1-GTP (%)
Control
TTX
NS-1619
D
Cellular Rac1-GTP (%)
Control
TTX (30 µM)
E
Rac1-GTP
Rac1
DAPI
Merge
Control
TTX
NS-1619
20 µm
F
Control
TTX
NS-1619
Total Rac1 (relative)
Radius (µm)
G
Peak Rac1 (%)
Control
TTX
NS-1619
H
Rac1-GTP/Rac1
Control
TTX
NS-1619

Figure 8

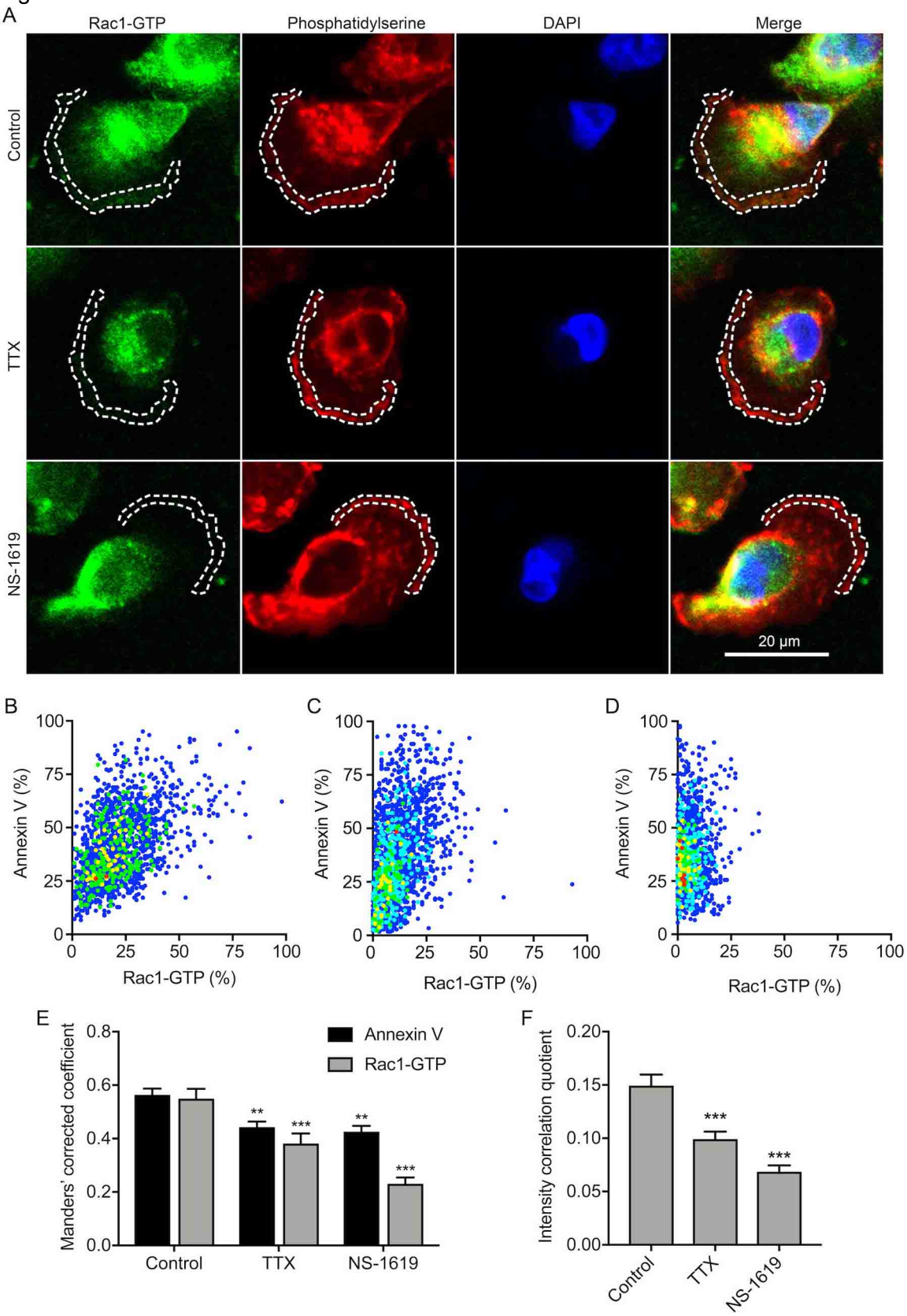
A
Rac1-GTP
Phosphatidylserine
DAPI
Merge
Control
TTX
NS-1619
20 µm
B
C
D
Annexin V (%)
Rac1-GTP (%)
0
25
50
75
100
E
Manders' corrected coefficient
0.0
0.2
0.4
0.6
0.8
Annexin V
Rac1-GTP
**
***
Control
TTX
NS-1619
F
Intensity correlation quotient
0.00
0.05
0.10
0.15
0.20
***

Figure 9

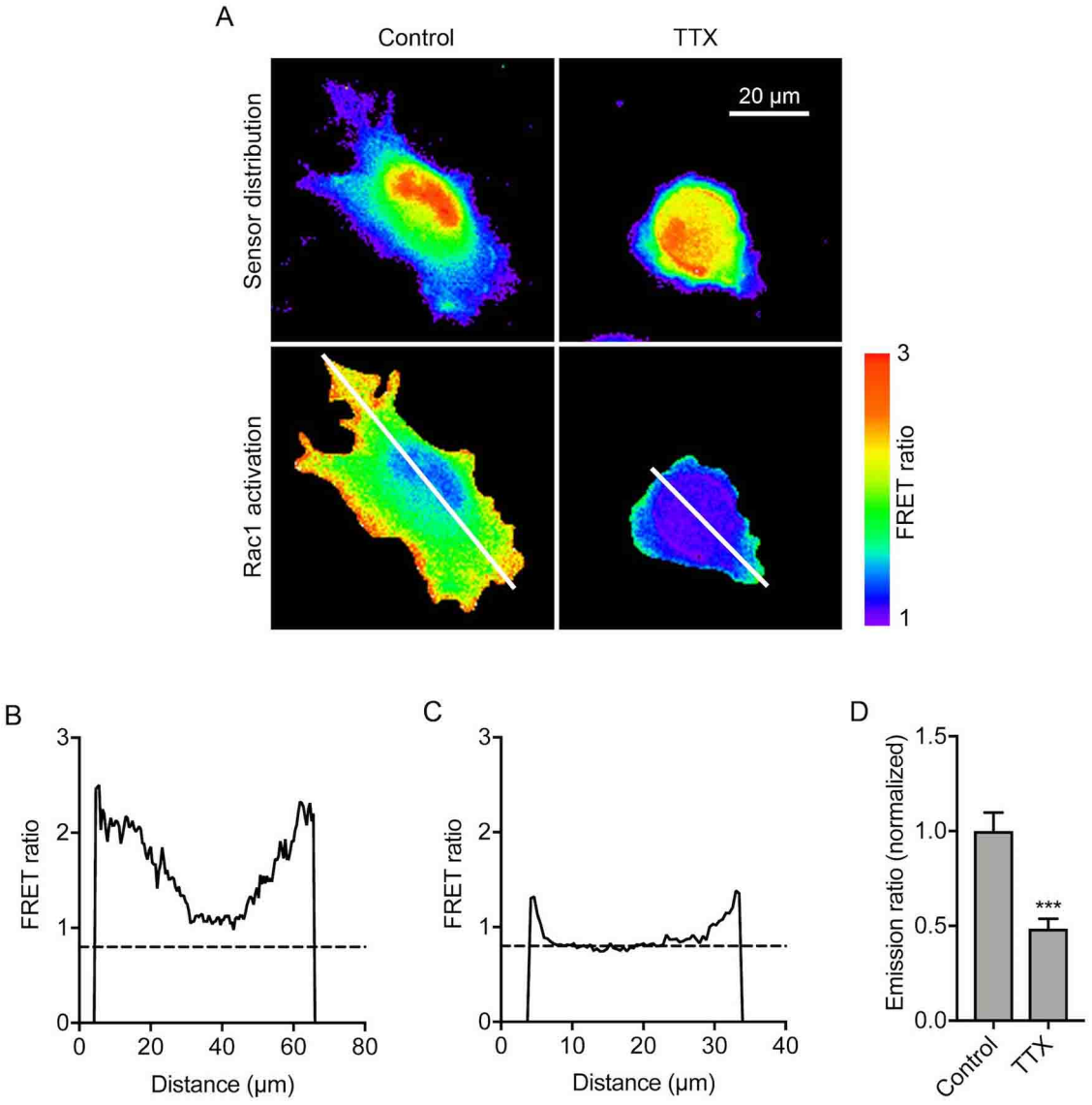
A
Control
TTX
20 µm
Sensor distribution
Rac1 activation
3
FRET ratio
1
B
FRET ratio
Distance (µm)
C
FRET ratio
Distance (µm)
D
Emission ratio (normalized)
***
Control
TTX

Figure 10

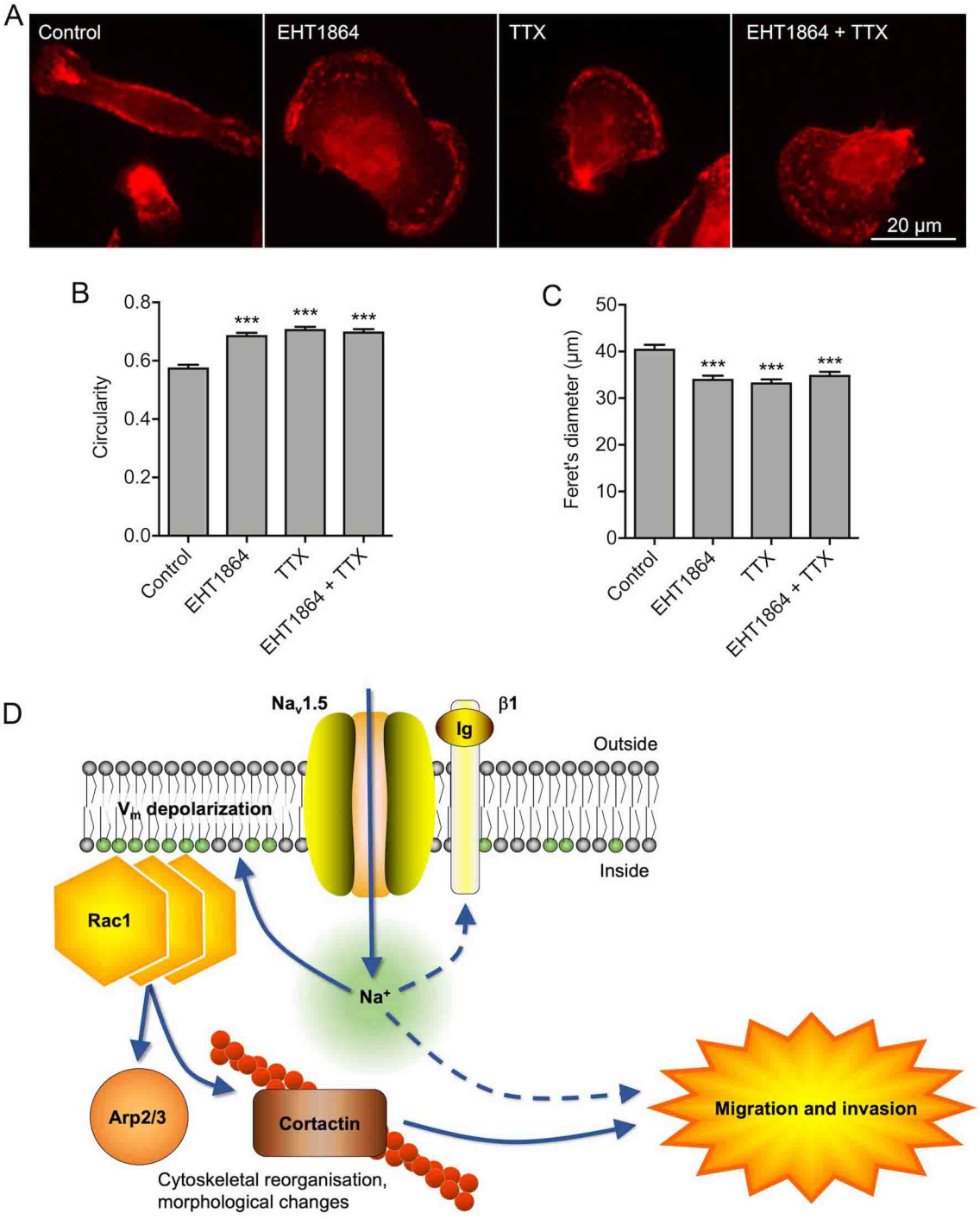
A
Control
EHT1864
TTX
EHT1864 + TTX
20 µm
B
Circularity
0.8
0.6
0.4
0.2
0.0
***
Control
EHT1864
TTX
EHT1864 + TTX
C
Feret's diameter (µm)
50
40
30
20
10
0
D
Na$_v$1.5
β1
Ig
Outside
Inside
V$_m$ depolarization
Rac1
Na$^+$
Arp2/3
Cortactin
Cytoskeletal reorganisation,
morphological changes
Migration and invasion